Theory of Non-Dimensional Groups in Film Effectiveness Studies

Francesco Ornano
Department of Engineering Science,
University of Oxford,
Parks Road,
Oxford OX1 3PJ, UK
e-mail: francesco.ornano@eng.ox.ac.uk

Thomas Povey[1]
Department of Engineering Science,
University of Oxford,
Parks Road,
Oxford OX1 3PJ, UK
e-mail: thomas.povey@eng.ox.ac.uk

The desire to improve gas turbines has led to a significant body of research concerning film cooling optimization. The open literature contains many studies considering the impact on film cooling performance of both geometrical factors (hole shape, hole separation, hole inclination, row separation, etc.) and physical influences (effect of density ratio (DR), momentum flux ratio, etc.). Film cooling performance (typically film effectiveness, under either adiabatic or diabatic conditions) is almost universally presented as a function of one or more of three commonly used non-dimensional groups: blowing—or local mass flux—ratio, density ratio, and momentum flux ratio. Despite the abundance of papers in this field, there is some confusion in the literature about the best way of presenting such data. Indeed, the very existence of a discussion on this topic points to lack of clarity. In fact, the three non-dimensional groups in common use (blowing ratio (BR), density ratio, and momentum flux ratio) are not entirely independent of each other making aspects of this discussion rather meaningless, and there is at least one further independent group of significance that is rarely discussed in the literature (specific heat capacity flux ratio). The purpose of this paper is to bring clarity to this issue of correct scaling of film cooling data. We show that the film effectiveness is a function of 11 (additional) non-dimensional groups. Of these, seven can be regarded as boundary conditions for the main flow path and should be matched where complete similarity is required. The remaining four non-dimensional groups relate specifically to the introduction of film cooling. These can be cast in numerous ways, but we show that the following forms allow clear physical interpretation: the momentum flux ratio, the blowing ratio, the temperature ratio (TR), and the heat capacity flux ratio. Two of these parameters are in common use, a third is rarely discussed, and the fourth is not discussed in the literature. To understand the physical mechanisms that lead to each of these groups being independently important for scaling, we isolate the contribution of each to the overall thermal field with a parametric numerical study using 3D Reynolds-averaged Navier–Stokes (RANS) and large eddy simulations (LES). The results and physical interpretation are discussed. [DOI: 10.1115/1.4046277]

Keywords: computational fluid dynamics (CFD), heat transfer and film cooling

Introduction

In a simple analysis of the gas turbine—in which the impact of cooling flows is neglected—for a given compression ratio and compressor outlet temperature, overall thermal efficiency increases with increasing turbine entry temperature (TET). Using more sophisticated analyses, which count the impact of cooling flows, is possible to show that the efficiency gain associated with higher TET is quite modest for a given material temperature capability. This is because of the thermal and aerodynamic cycle penalties associated with internal and film cooling. Thus, notwithstanding improvements in material technology, much of the effort in high pressure (HP) turbine optimization surrounds aero-thermal optimization of the cooling system.

The vast majority of experimental work, and indeed a considerable proportion of computational work, is conducted at physical conditions that are different from the engine (typically lower temperature and pressure). It is rare in these studies for all relevant non-dimensional groups to be simultaneously matched to engine conditions. Compromises, therefore, have to be made in the scaling of experiments. Despite the significant body of work on this topic, there is still discussion in the literature about the best way of scaling film effectiveness experiments and data. In some cases, the non-independence of certain redundant non-dimensional groups is neglected, making the discussion of the relative importance of these groups somewhat meaningless. Other independent groups are often ignored, leading to scaling differences that mean the simulated system is only a partial representation of the engine situation.

The purpose of this paper is to bring clarity to the full set of non-dimensional groups required for engine similarity in experiments or numerical simulations of film cooling, explain the physical significance of each group, and quantify the error introduced when only partial scaling is achieved.

Literature Relating to Dimensional Analysis of Film Cooling Effectiveness Problems. In laboratory experiments, absolute pressure and temperature (and other parameters) generally take very different values from engine conditions. Tests are performed at scaled conditions, whereby non-dimensional groups are matched between laboratory and engine environments. There is a certain degree of arbitrariness with which groups are chosen, so the question arises: *which are the best non-dimensional groups to choose?*

In the open literature, film effectiveness data are most commonly presented as a function of one of three common non-dimensional groups: blowing ratio (BR), momentum flux ratio, and density ratio (DR). In the vast majority of studies, changes in the operating conditions of the experiment do not allow independent variation of each of these three groups. Thus, although trends in film effectiveness are often attributed to a small number of physical processes

[1]Corresponding author.

Contributed by the Heat Transfer Division of ASME for publication in the Journal of Turbomachinery. Manuscript received April 29, 2019; final manuscript received January 24, 2020; published online February 10, 2020. Assoc. Editor: Dr. Jeffrey Bons.

that have been repeatedly observed in studies, the individual sensitivities are—strictly speaking—impossible to determine. Relatively few papers discuss this point, and there is almost no literature which both strictly examines both the dimensional analysis problem and relates the result of that examination (proposed groups) to film effectiveness trends in which true de-coupling was achieved (groups being varied individually, one at a time).

In this section, we review the most relevant literature relating to this combined problem, i.e., the subject of this paper.

A similarity analysis of model experiments for film cooling was presented by Eckert [1], who noted that similarity between model tests and engine conditions is achieved when the dimensionless velocity, pressure, and temperature fields are matched. In order to obtain this, a number of dimensionless parameters have to be matched.

Baldauf and Scheurlen [2] presented a similarity analysis for film cooling to isolate the parameters of influence related to geometry and flow properties. They reduced the number of parameters of influence for the physical problem (referencing analysis presented by Eckert) and investigated the effect of these parameters. In their study, they considered the same gas (air) for mainstream and coolant.

Luque et al. [3] presented a scaling theory for overall cooling effectiveness based on a recovery and redistribution temperature, which includes the effect of coupling compressible effects in the mainstream flow with the incompressible internal cooling channel, via through wall heat transfer (concept of "redistribution" of compressible effects, even into the incompressible domain). In their study, they defined 13 non-dimensional groups on which the conjugate heat transfer situation with film cooling for a vane suction side depends. The purpose was to define an overall metal effectiveness (including the effect of internal cooling) parameter relevant to compressible flow situations and to determine the groups which it was a function of.

Literature Relating to Practice for Using Non-dimensional Groups to Represent Film Cooling Effectiveness Data From Experiments. Non-dimensional parameters in common use in the literature to represent film performance characteristics are blowing (or mass flux) ratio, BR; momentum flux ratio, I; and DR.

The impact of blowing ratio and density ratio on film cooling was investigated by Sinha et al. [4]. They showed that at low blowing ratios (i.e., low local mass flux ratios), the jet was attached to the surface and the centerline film effectiveness was primarily a function of the blowing ratio; for higher blowing ratios, the jet detached (and potentially reattached) and the film effectiveness was also strongly dependent on the density ratio (because of its effect on momentum flux ratio).

Thole et al. [5] described the momentum flux ratio as the appropriate parameter to characterize the flow structure (attached, separated, etc.) of the cooling jet close to the hole. Haas et al. [6] agreed that the penetration of a jet is mainly a function of the momentum flux ratio and injection angle (their study included different geometries).

Thole et al. [5] defined the range of momentum flux ratio for which a row of cylindrical jets (with 35 deg inclination angle) was separated or attached. They found that a complete jet detachment occurred for $I > 0.8$, whereas a fully attached jet was found for $I < 0.4$. In the range $0.4 < I < 0.8$, cooling jets were found to separate and subsequently reattach. In their review paper, Bogard and Thole [7] observed similar effects.

Pedersen et al. [8] measured the film effectiveness downstream of a row of cylindrical jets for different density ratios. At low BR = 0.2, they found that the film effectiveness was approximately constant for density ratios in the range DR = 0.8–4. The conclusion was that at this BR, the jets were well attached to the wall and the film effectiveness was primarily a function of BR. At higher BR, they showed that better film effectiveness was reached for higher DR, at fixed BR. This was attributed to the reduced tendency of the jets to separate, due to lower momentum flux associated with higher density ratio.

Shiau et al. [9] carried out an experimental work to study endwall film effectiveness distributions on an annular nozzle guide vane (NGV) sector with laidback fan-shaped and cylindrical holes using the pressure-sensitive paint technique. The test matrix included experiments at three values of the mass flow ratio, each of them at two different density ratios. They concluded that the lateral coverage was improved by increasing the density ratio, for a given mass flow ratio. This was attributed to the reduced momentum flux ratio. Prost and Acharya [10] performed temperature and heat flux measurements in a film-cooled, heated cascade of nozzle guide vanes. Tests were conducted for three values of the blowing ratio, each of them at three values of the density ratio. They found that jets spreading was improved for higher DR. This was attributed to reduced momentum flux ratio.

Some studies, such as by Vinton et al. [11], report results from a single cylindrical and fan-shaped hole, as a function of three parameters: blowing ratio, density ratio, and momentum flux ratio. They compared two tests at the same momentum flux ratio and different density ratios (DR = 1 and DR = 4). Differences in the lateral spreading of the jet were observed: the higher density (DR = 4) jet had improved lateral spreading in the near-hole region and reduced film effectiveness on the downstream region compared with the lower density ratio case (DR = 1). This may be attributed to greater mass flux. Recent works on scaling parameters have been presented by Rutledge and Polanka [12] and Rutledge et al. [13]. They performed a computational study to evaluate the effect of a number of scaling parameters on adiabatic film effectiveness and heat transfer coefficient for a single hole located on a turbine blade leading edge. Results indicated that thermal properties such as heat capacity and thermal viscosity are important when scaling experimental work to engine-representative conditions. They describe the importance of momentum flux ratio for predicting the trajectory of the film and of heat capacity ratio for the level of film effectiveness. Greiner et al. [14] computationally investigated the non-dimensional parameters important when scaling from ambient to engine temperatures. They found that, in addition to blowing ratio, momentum flux ratio, and density ratio, the mainstream and coolants Reynolds numbers should be matched for accurate scaling of film performance. When matching BR, I, DR, and Pr, between ambient experimental conditions and engine temperatures, the simultaneous matching of both mainstream and coolant Reynolds numbers was, however, not possible. The authors found that matching the coolant Reynolds number led to an improved match between the two situations.

In summary, we find the following from reviewing the literature in this area:

(i) there is good agreement about the importance and physical significance of momentum flux ratio as the dominant parameter for aerodynamics, or jet trajectory, in the near-hole region;
(ii) there is confusion in a considerable number of papers of the interrelationship of blowing ratio, density ratio, and momentum flux ratio. These parameters are not—from the point of view of similarity—truly independent, and discussion should not imply they are;
(iii) there is very limited awareness—and then only in very recent papers—of the importance of specific heat capacity ratios on film effectiveness;
(iv) most discussions of scaling are somewhat partial, in that a complete set of independent non-dimensional groups and a discussion of their relative importance in experiments with incomplete scaling appears not to have been presented;
(v) the physical significance/interpretation of scaling parameters is rarely discussed;
(vi) there is some confusion over the complete independent set of scaling parameters, how they arise, and how best to choose a set which allows clear physical interpretation of film cooling data.

The purpose of this paper is to bring additional clarity to the problem of defining the correct scaling parameters for film cooling data, understand sensitives in a properly controlled (orthogonally separated) numerical study, and add physical interpretation of each parameter so its individual effect may be better understood.

Dimensional Analysis

For the situation of a film-cooled adiabatic wall, there are 16 physical quantities that define the problem

$$p_{01}, T_{01}, c_{p1}, \gamma_1, \mu_1, k_1, p_{02}, T_{02}, c_{p2}, \gamma_2, \mu_2, k_2, p, T_w, s, L \quad (1)$$

where p_0, T_0, c_p, γ, μ, k, p, T_w, s, and L are the total pressure, total temperature, heat capacity, isentropic exponent, dynamic viscosity, thermal conductivity, static pressure, wall temperature, surface streamwise coordinate, and the characteristic length downstream the cooling holes, respectively. The subscripts 1 and 2 refer to mainstream and coolant conditions, respectively. Figure 1 shows the physical situation and parameters of influence.

The problem contains four dimensions (mass, length, temperature, and time) and we therefore expect—by the Buckingham Pi theorem—that not less than 12 non-dimensional groups will be required to fully describe the system. That is

$$\pi_{12} = f(\pi_1, \pi_2, \ldots, \pi_{11}) \quad (2)$$

Making film effectiveness the subject, a dimensional analysis confirms the possibility of the following form

$$\frac{T_{01} - T_w}{T_{01} - T_{02}} = f\left(\frac{p_{02} - p}{p_{01} - p}, \frac{\gamma_2}{\gamma_1}\frac{\gamma_1 - 1}{\gamma_2 - 1}, \frac{c_{p2}}{c_{p1}}, \frac{T_{02}}{T_{01}}, \frac{\mu_2}{\mu_1}, \frac{k_2}{k_1}, \frac{s}{L}, \mathrm{Re}_1, \mathrm{Pr}_1, M_1, \gamma_1\right) \quad (3)$$

where the subject is $\pi_{12} = \eta$. The remaining terms will be discussed later in the text. Here, we have taken as direct a route as possible from the underlying variables and cast the non-dimensional groups in the simplest possible form.

We now seek to manipulate certain groups into forms which are recognizable (e.g., blowing ratio, momentum flux ratio, etc.) or into forms which we believe have clear physical interpretation (e.g., temperature ratio, specific heat capacity flux ratio, etc.)

For incompressible flow, the momentum flux ratio can be expressed as follows:

$$I \equiv \frac{\rho_2 u_2^2}{\rho_1 u_1^2} = \frac{p_{02} - p}{p_{01} - p} = \pi_1 \quad (4)$$

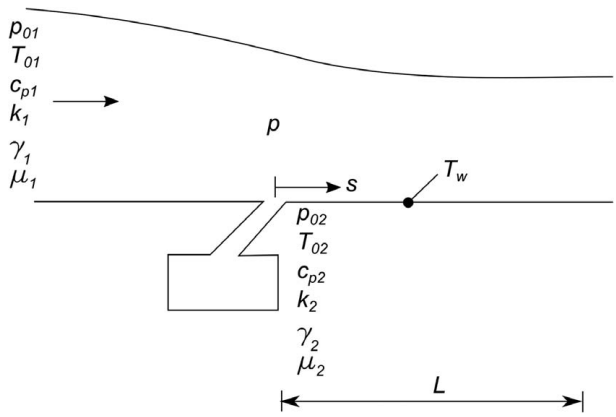

Fig. 1 Physical situation and parameters of interest for a film-cooled adiabatic wall

That is, the momentum flux ratio is interchangeable with the first group in Eq. (3).

Noting that for incompressible flow ($\rho \sim \rho_0$ and $T \sim T_0$)

$$\frac{\rho_2}{\rho_1} = \frac{p_{02}}{p_{01}}\frac{T_{01}}{T_{02}}\frac{c_{p1}}{c_{p2}}\frac{\gamma_2}{\gamma_1}\frac{\gamma_1 - 1}{\gamma_2 - 1} \quad (5)$$

we can write the blowing ratio (BR) in terms of the momentum flux ratio (I) and the density ratio as follows:

$$\mathrm{BR} \equiv \frac{\rho_2 u_2}{\rho_1 u_1} = \left(I\frac{\rho_2}{\rho_1}\right)^{1/2} = \left(\frac{p_{02}}{p_{01}}\frac{T_{01}}{T_{02}}\frac{c_{p1}}{c_{p2}}\frac{\gamma_2}{\gamma_1}\frac{\gamma_1 - 1}{\gamma_2 - 1}\frac{p_{02} - p}{p_{01} - p}\right)^{1/2} = \pi_2 \quad (6)$$

We replace $(\gamma_2/\gamma_1)(\gamma_1 - 1)/(\gamma_2 - 1)$ in Eq. (3) with the blowing ratio. The influence on the film performance of different heat capacities for mainstream gas and coolant gas is accounted for by the specific heat capacity flux ratio, E, which we defined by

$$E \equiv \frac{\rho_2 u_2 c_{p2}}{\rho_1 u_1 c_{p1}} = \mathrm{BR}\frac{c_{p2}}{c_{p1}} = \pi_3 \quad (7)$$

We replace c_{p2}/c_{p1} in Eq. (3) with the specific heat capacity flux ratio.

The last parameter of interest is the temperature ratio, defined by

$$\mathrm{TR} \equiv \frac{T_{02}}{T_{01}} = \pi_4 \quad (8)$$

which arises naturally in the dimensional analysis leading to Eq. (3).

The relationship implied by (3) is recast in the following 12 dimensionless groups

$$\frac{T_{01} - T_w}{T_{01} - T_{02}} = f\left(I, \mathrm{BR}, E, \mathrm{TR}, \frac{\mu_2}{\mu_1}, \frac{k_2}{k_1}, \frac{s}{L}, \mathrm{Re}_1, \mathrm{Pr}_1, M_1, \gamma_1\right) \quad (9)$$

The first four groups on the right-hand side have been discussed

$$\begin{aligned} \pi_1 &= I = \frac{p_{02} - p}{p_{01} - p} \\ \pi_2 &= BR = \left(\frac{p_{02}}{p_{01}}\frac{T_{01}}{T_{02}}\frac{c_{p1}}{c_{p2}}\frac{\gamma_2}{\gamma_1}\frac{\gamma_1 - 1}{\gamma_2 - 1}\frac{p_{02} - p}{p_{01} - p}\right)^{1/2} \\ \pi_3 &= E = BR\frac{c_{p2}}{c_{p1}} \\ \pi_4 &= TR = \frac{T_{02}}{T_{01}} \end{aligned} \quad (10)$$

Groups π_5 and π_6 relate to fluid property ratios between the mainstream and coolant gas

$$\pi_5 = \frac{\mu_2}{\mu_1}, \qquad \pi_6 = \frac{k_2}{k_1} \quad (11)$$

Group π_7 is the non-dimensional surface length

$$\pi_7 = \frac{s}{L} \quad (12)$$

Groups π_8, π_9, and π_{10} are the Reynolds number, Prandtl number, and Mach number for the mainstream flow

$$\pi_8 = \mathrm{Re}_1 = \sqrt{\frac{2R_1T_1(p_{01}-p)}{p}}\frac{L}{\mu_1}$$
$$\pi_9 = \mathrm{Pr}_1 = \frac{\mu_1 c_{p1}}{k_1} \tag{13}$$
$$\pi_{10} = M_1 = \frac{\sqrt{2(p_{01}-p)}}{\sqrt{\gamma_1}}$$

The mainstream Reynolds number (π_8) and Mach number (π_{10}) are expressed in incompressible form because the mainstream Mach number was held constant and was in the incompressible regime. The additional effect of compressibility was not investigated in this study, but its inclusion would make an interesting topic for an extension to this work. Reynolds number based on mainstream velocity and hole diameter was approximately 1.8×10^3. This was constant throughout the study.

Group π_{12} is the subject, the adiabatic film effectiveness

$$\pi_{12} = \frac{T_{01}-T_w}{T_{01}-T_{02}} = \eta \tag{14}$$

The dimensionless groups are by definition orthogonal and can be varied independently to study the effect of each of them on film effectiveness. In particular, we are interested in groups π_1 to π_4. We believe these to be the dominant groups in relationship (9) (recast from relationship (3)), and also to be amenable to physical interpretation.

To isolate the sensitivity of $\pi_{12} = \eta$ to groups π_1 to π_4, we construct a numerical experiment in which we individually vary one of the groups π_1 to π_4, while keeping all the remaining groups (π_1 to π_{11}) constant. Thus, four studies are set up in which we study the impact of groups π_1 to π_4 in isolation.

The 11 independent groups in Eq. (9) have a non-linear relationship with the 15 independent variables (on which T_w depends) of Eq. (1)

$$p_{01}, T_{01}, c_{p1}, \gamma_1, \mu_1, k_1, p_{02}, T_{02}, c_{p2}, \gamma_2, \mu_2, k_2, p, s, L$$

Our object in each of the four studies is to maintain ten of the groups (π_1 to π_{11}) constant while varying one of π_1 to π_4. Examining the equations, we determine that this is possible for fixed values of the following input variables

$$p_{01}, T_{01}, c_{p1}, \gamma_1, p, s, L \tag{15}$$

These fixed independent variables were not changed during our study. The remaining independent variables

$$p_{02}, T_{02}, c_{p2}, \gamma_2, \mu_1, \mu_2, k_1, k_2 \tag{16}$$

were regarded as free independent variables in our study and were adjusted to achieve the required test matrix of π_1 to π_{11}.

The free independent variables in Eq. (16) were solved iteratively in MATLAB by using the function lsqnonlin. The combined variable sets (7 fixed, 8 free) were used as boundary conditions for computational fluid dynamics (CFD) simulations. The outputs from the CFD simulations were the adiabatic wall temperature distributions T_w, representing the dependent group in the study ($\pi_{12} = \eta$).

Region-Specific Scaling Parameters

In this section, we introduce the concept that the relative importance of scaling parameters is region-specific (with respect to the cooling hole). That is, the dominant independent groups depend on the location with respect to the cooling hole. We introduce the definitions of the *binary region* (near hole), *intermediate region*, and *mixed-out region*. These regions are used in the analysis section later in this paper.

Binary Region. The binary region, or near-hole region, is the part of the flow in which the films are *substantially unmixed*. This is identified by a locally binary distribution of the film effectiveness (values close to 0, 1). In this region, the circumferential (line) average can take any value and depends on the local aerodynamics, film cooling hole spacing, etc. For a given geometry, the flow structure (jet trajectory, and to a lesser extent the jet mixing rate) is primarily controlled by the momentum flux ratio. The most obvious structural difference is between an attached and a separated jet, but more generally, the momentum flux ratio determines the jet trajectory.

It is argued in the binary region the dominant scaling parameter local for film effectiveness is the momentum flux ratio, because it is the most important parameter for the aerodynamic similarity between scaled physical situations.

Mixed-Out Region. We define the mixed-out region to be the region far downstream of the hole where the circumferential variation of film effectiveness is small in comparison with the circumferential average value of film effectiveness. We arbitrarily take a value for the ratio of variation to an average value of 0.2.

In this region, we argue that the mixed-out film effectiveness depends primarily on the balance of heat storage capacity of the coolant and mainstream. We believe that similar mixing can be assumed in many real situations (in which other independent groups are changed), because far downstream of the hole the mixing is dominated by the mainstream turbulence and not by, for example, near-hole flow structure differences or turbulence differences caused by changes in coolant momentum flux ratio.

In the mixed-out region, the dominant scaling parameter for film effectiveness is the specific heat capacity flux ratio, E, because this represents the relative heat storage capacity of the coolant and mainstream flows.

Intermediate Region. We define the intermediate region more loosely to be the region between the binary region (approximately binary values of film effectiveness) and the mixed-out region (low circumferential variation in film effectiveness). In the intermediate region, films are partially mixed and the film effectiveness is neither entirely dependent on momentum flux ratio (due to the primary dependence on flow structure) nor specific heat capacity flux ratio (due to the primary dependence on heat storage capacity). In this transition region, the behavior is complex and significantly dependent on more than one of the key scaling groups.

Figure 2 shows the CFD domain used in this study, with the locations of the binary, intermediate, and mixed-out post-processing lines, at 0, 24, and 48 diameters downstream of the holes, respectively. The domain includes 15 cooling holes with a spacing-to-diameter ratio of 2 and a fixed hole inclination of 30 deg.

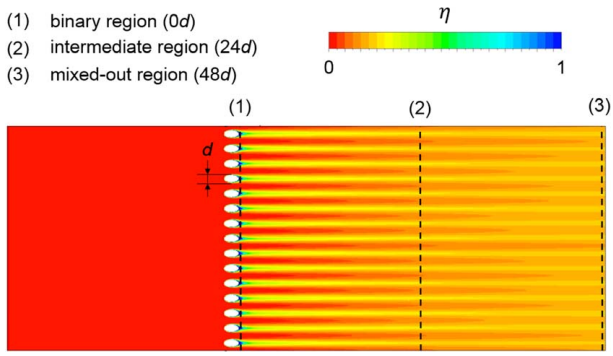

Fig. 2 CFD domain showing the binary, intermediate, and mixed-out post-processing lines

Test Matrix

The CFD experiments were designed to investigate the independent effect of changing π_1, π_2, π_3, and π_4 (I, BR, E, and TR). For each group π_1 to π_4, ten values around a nominal design point were investigated while maintaining the remaining ten of the independent groups (of π_1 to π_{11}) constant. The nominal values were $I = 1.000$, $\text{BR} = 1.000$, $E = 1.000$, and $\text{TR} = 0.800$. The nominal value for the temperature ratio was set to $\text{TR} = 0.800$ to allow film effectiveness to be defined in terms of the temperature at the adiabatic surface (noting errors where temperature differences become too small).

Numerical Methods for RANS Simulations

Solver Settings. The numerical analysis was performed using ANSYS-CFX (selected for ease of implementing additional transport equations), with Reynolds Averaged Navier–Stokes (RANS) settings and high-resolution discretization (second-order accurate) for both advection and turbulence terms. The k–ω shear stress transport (SST) turbulence model with automatic wall functions and reattachment prediction model was used. The flow conditions were incompressible.

Mesh and Boundary Conditions. The computational domain is shown in Fig. 3(*a*). Meshing was performed using BOXERMesh. The domain included a single row of 15 cylindrical cooling holes fed by a single coolant plenum. The choice of cylindrical holes was somewhat arbitrary: in this work, we are concerned with fundamental physical processes, and not characterizations for a particular geometry. The cooling holes had an inclination of 30 deg with respect to the horizontal plane and a diameter of 2 mm. The hole spacing was $2d$ (where d is the hole diameter). Mesh interfaces at the cooling hole inlets were managed using the general grid interface (GGI) option to allow individual cooling hole mass flowrates to be determined during post-processing. The mesh had approximately 5.2 million hybrid cells (hexahedral and tetrahedral). In the near-wall region, the grid was refined with 15 prism layers with an expansion ratio of 1.2. The value of the non-dimensional wall distance (z^*) was approximately 1 on most of the wetted surfaces, with only some localized areas having a maximum value below 5. Figure 3(*b*) shows the detail of the cooling hole mesh.

The inflow boundary condition was imposed at the domain inlet, with specified total pressure, total temperature, flow direction (normal to the inlet boundary), and turbulence intensity ($Tu = 10\%$). A value of static pressure was imposed at the domain outlet. The coolant was fed from the plenum, with fully meshed cooling holes (Fig. 3(*b*)). Uniform total pressure and total temperature were specified at the plenum inlet. The sides of both the main passage and the plenum domain were set to be periodic.

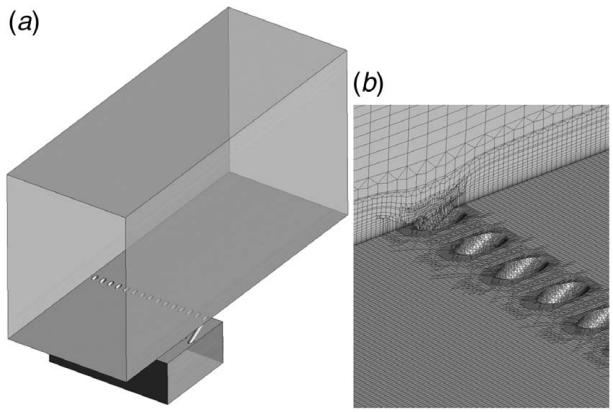

Fig. 3 Computational domain (*a*) and detail of the cooling hole mesh (*b*) used for RANS simulations

For the 40 computational experiments in this study, the mainstream and coolant gas properties were varied to set relevant values of non-dimensional groups. This was done using the preprocessing routine CFX-Pre. Recall that our object in each of the four studies is to maintain ten of the groups (π_1 to π_{11}) constant while varying one of π_1 to π_4. The fixed independent variables were p_{01}, T_{01}, c_{p1}, γ_1, p, s, L (Eq. (15)), and the free independent variables were p_{02}, T_{02}, c_{p2}, γ_2, μ_1, μ_2, k_1, k_2 (Eq. (16)). Defining the test matrix was not entirely trivial, and the authors are willing to make it available on request for future studies. The coolant flow was simulated as a foreign gas, with a molar fraction of 1.0 at the coolant plenum inlet and 0.0 at the mainstream domain inlet. Thus, coolant properties could be varied independently of the mainstream gas. The CFD solution was performed by considering an additional transport equation for the coolant fluid.

Grid Independency Study. A grid independency study was performed in order to select the minimum adequate mesh resolution to capture all significant flow features. The domain was solved with four levels of grid refinement on the cooled wall: M1, M2, M3, and M4, with total element counts 4.3×10^6, 4.7×10^6, 5.2×10^6, and 7.2×10^6, respectively. The grid refinement was performed by halving the edge length of the squared cells close to the cooled wall for each refinement level. That is, most of the cells were added in the near-wall region. The test conditions were $E = I = \text{BR} = 1.000$ and $\text{TR} = 0.800$. The results were compared in terms of the lateral distribution of film effectiveness in the binary ($x = 0d$), intermediate ($x = 24d$), and mixed-out ($x = 48d$) regions. Figure 4 shows the results of the grid independency study. Approximate grid independency was achieved for 5.2×10^6 elements (mesh M3 in Fig. 4) for all the three regions. This mesh resolution was chosen for the RANS calculations in the current study.

Numerical Methods for Large Eddy Simulations

Due to the large design space of the parametric study presented in this paper, RANS simulations were used for the majority of the study and captured many of the important aspects of the flow mixing despite being based on turbulence models rather than direct simulation. To explain more complex local mixing

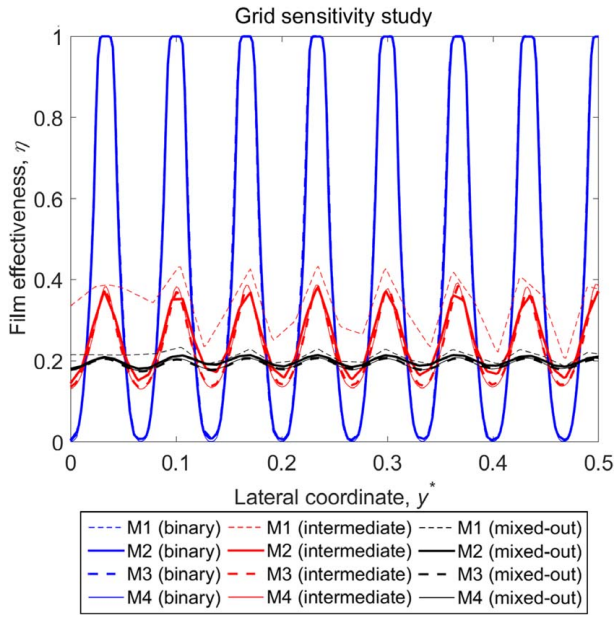

Fig. 4 Film effectiveness distribution in the binary, intermediate, and mixed-out regions obtained during the grid sensitivity study. The test conditions were $E = I = \text{BR} = 1.000$ and $\text{TR} = 0.800$.

phenomena, higher-fidelity large eddy simulations (LES) were used to complement the RANS simulations where necessary.

Solver Settings. The LES sub-grid wall-adapting local eddy-viscosity model [15] was used for the present work. This is based on a tensor invariant and reproduces the proper eddy-viscosity scaling at the wall. It is recommended for complex geometries as no explicit filtering is needed, and only local information is required to determine the eddy-viscosity. It is also known for its accuracy in predicting small turbulent structures (due to modeling of the strain and the rotation rate [15]). A second-order discretization in space and time was selected for the present study. As for the RANS setup, the fluid domain was simulated by using two gas species: mainstream gas and coolant. An additional transport equation for the mainstream gas was solved each iteration and the coolant mass fraction was directly computed from its solution. The mainstream mass fraction was set to 1.0 at the domain inlet and to 0.0 at the plenum inlet. The ideal gas law was selected for the equation of state. The flow conditions were incompressible.

The validation of both RANS and LES models employed in this study is presented in Appendix C.

Mesh Resolution for Large Eddy Simulations Study. An additional computational domain was meshed for the LES including only three cooling holes. This choice was made in order to avoid any imposed lateral periodicity, and therefore to allow real (stochastic) interaction between jets in the lateral direction. The entire volume mesh was highly refined, with enhanced resolution from the wall up to $5d$ in the direction perpendicular to the wall, and spanning the entire axial length of the domain. The global mesh had 17 million hybrid (tetrahedral/hexahedral) cells, as shown in Fig. 5. Particular attention was paid on the near-wall region, which had 15 prism layers in the boundary layer region with an expansion ratio of 1.2. The value of the non-dimensional distance from the wall based on the Reynolds number (Δz^+) was kept less than 1 over the entire cooled wall and cooling hole surfaces. The grid spacing on the x (streamwise) and y (lateral) directions were set to be Δx^+, $\Delta y^+ < 10$, as recommended by Tyacke and Tucker [16] on LES best practice.

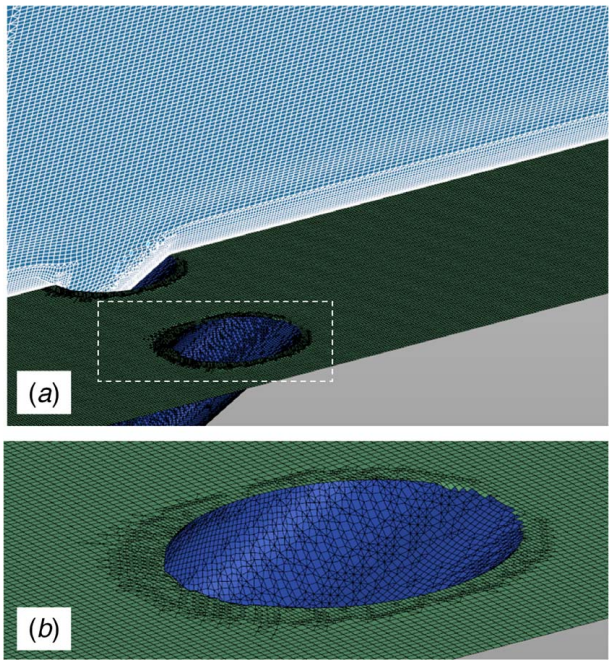

Fig. 5 Computational mesh employed for LES simulations: (*a*) slice of volume mesh and (*b*) detail of the cooling hole grid

The level of refinement of the mesh close to the wall was set to the order of the Kolmogorov microscale for length, $\eta = (\nu^3/\varepsilon)^{1/4}$, the scale below which energy is dissipated primarily by viscous forces. Following the methodology suggested in Ref. [17], parallel steady simulations were used to estimate the value of turbulent eddy dissipation rate, ε. The Kolmogorov microscale was found to be approximately $\eta = 2.35 \times 10^{-5}$m. The mesh size for the layer closest to the cooled wall was set smaller than the Kolmogorov microscale for length, with the first cell height being $\Delta z_1 = 1.5 \times 10^{-5}$m. The resolved energy spectrum is given in Frequency Analysis section.

Choice of Time Step. In cross-flows, the Strouhal number typically takes a value of approximately 0.2 (Lin et al. [18]). The corresponding vortex shedding frequency is calculated as follows:

$$f = \mathrm{St}\, U/D \sim 0.2\, U/D \tag{17}$$

where D is the hole diameter and U is the freestream velocity magnitude. Considering the current geometry and flow conditions, a shedding frequency of approximately 3.4 kHz is estimated. In order to obtain enough resolution to resolve the unsteady flow features, a time-step of 10^{-5} s was selected for the present study.

Frequency Analysis. Figure 6(*a*) shows the amplitude spectrum obtained by performing a fast Fourier transform (FFT) of the velocity signal acquired with a monitor point located approximately $1.0d$ downstream the centerline of the central cooling hole and approximately $0.25d$ from the wall. The velocity frequency spectrum is dominated by a peak at 3.5 kHz, very close to the vortex shedding frequency predicted based on the typical Strouhal number for jets in cross-flow.

The power density spectrum (PSD) of the velocity time-signal is depicted in Fig. 6(*b*) as a function of the frequency, f. At low frequencies ($f < 1$ kHz), the energy is associated with the largest eddies which typically are dependent on the geometry of the domain. At higher frequencies ($1 < f < 10$ kHz), the spectrum is defined by the *inertial subrange*, identified by the relationship $E(f) \propto f^{-5/3}$. The eddies in this region have the highest energy content. The smallest eddies, which are responsible for the majority of viscous dissipation, occur at the highest frequencies ($f > 10$kHz). Figure 6(*b*) shows that the LES results were able to predict the inertial subrange (by direct comparison with the slope equal to −5/3 in this region), and the most relevant flow features were therefore fully resolved.

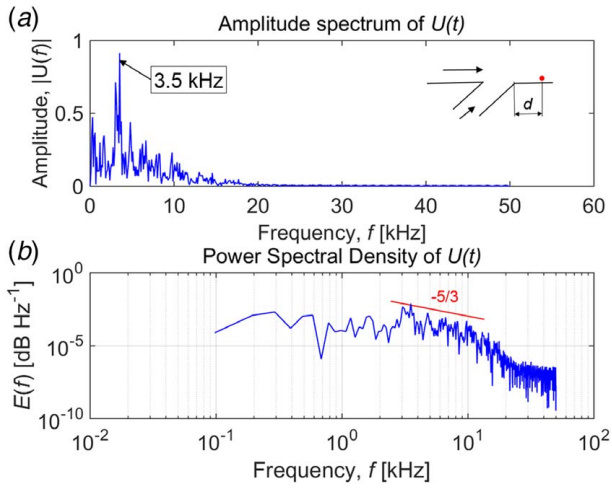

Fig. 6 (*a*) Fast Fourier transform and (*b*) power density spectrum of the transient velocity signal downstream the central cooling hole

Results and Discussion

In this section, we discuss the significance of the key non-dimensional groups in turn, and in particular consider how the relative importance of these groups differs in the binary, intermediate, and mixed out regions of the flow. First, we consider the momentum flux ratio, I.

Momentum Flux Ratio. In the region close to the cooling holes (the binary region), the coolant jets are substantially unmixed and the film effectiveness has a binary-like distribution assuming values close to either 0 or 1. In this region, the film effectiveness distribution has a strong dependence on the momentum flux ratio, because this controls the aerodynamic state of the jets, i.e., the coolant trajectory and shape of the jet.

Figure 7 shows RANS results for the lateral distribution of film effectiveness on the binary region as a function of the momentum flux ratio (in the range $0.500 < I < 2.000$). The normalized lateral coordinate y^* is defined as $y^* = (y - y_{min})/(y_{max} - y_{min})$. The film effectiveness decreases with increasing momentum flux ratios as the region in which jets are detached increases as a proportion of the surface area.

Results for the intermediate region (at an axial location of $x = 24d$) are shown in Fig. 8. In this region, there is still significant dependence of the film effectiveness distribution on I. For increasing I, the peaks in film effectiveness are reduced from a value of approximately 0.4 to a value of approximately 0.2. This region is beyond the reattachment point, so the effect is likely associated with changes in mixing caused by different initial coolant trajectories.

Results for the mixed-out region ($x = 48d$) are shown in Fig. 9. In this region, the lateral film effectiveness distribution is essentially independent of I. The curves have a similar average value (approximately 0.18), and relatively similar variation from the mean. For constant specific heat capacity flux ratio, blowing ratio, and temperature ratio, the film effectiveness is insensitive to the momentum flux ratio in the mixed-out region.

Laterally averaged film effectiveness values for the three regions are shown Fig. 10, normalized with respect to the case with the

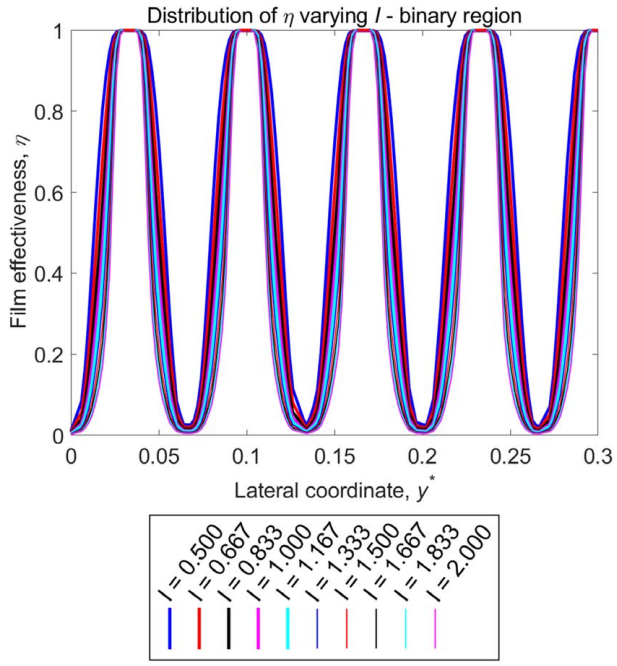

Fig. 7 Lateral distribution of film effectiveness in the binary region ($x = 0d$) as a function of the momentum flux ratio. Test conditions were $E = 1.000$, BR = 1.000, and TR = 0.800.

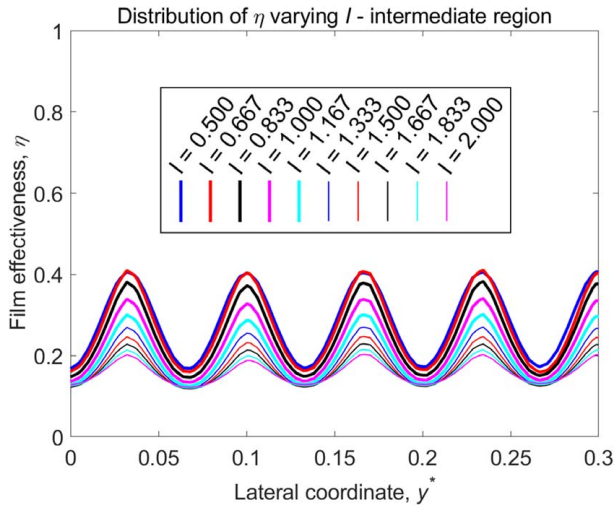

Fig. 8 Lateral distribution of film effectiveness on the intermediate region ($x = 24d$) as a function of the momentum flux ratio. Test conditions were $E = 1.000$, BR = 1.000, and TR = 0.800.

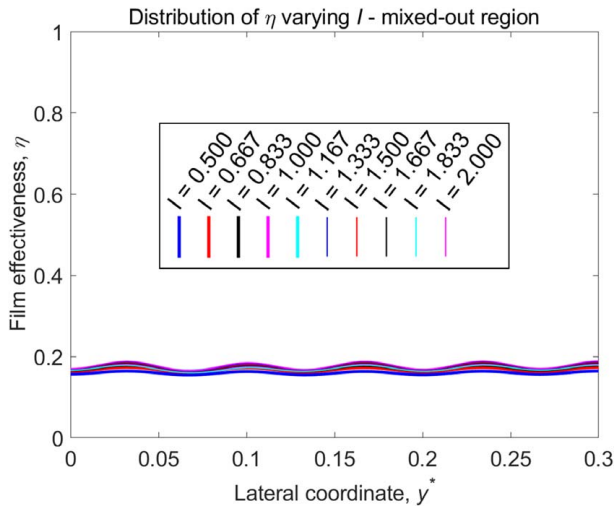

Fig. 9 Lateral distribution of film effectiveness on the mixed-out region ($x = 48d$) as a function of the momentum flux ratio. Test conditions were $E = 1.000$, BR = 1.000, and TR = 0.800.

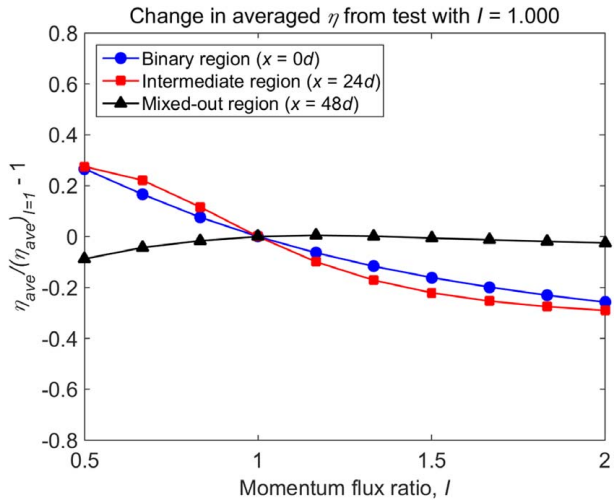

Fig. 10 Lateral average of film effectiveness as a function of I. Test conditions were $E = 1.000$, BR = 1.000, and TR = 0.800.

nominal momentum flux ratio $I = 1.000$. As discussed, the laterally averaged film effectiveness has a strong trend with I in both binary and intermediate regions (normalized variation from the baseline value of 0.25 to −0.25), indicating a large sensitivity to I in these regions. The sensitivity of the laterally averaged film effectiveness to I in the mixed-out region is considerably lower (−0.09 to +0.005).

In summary, the binary and intermediate regions show strong sensitivity of the laterally averaged film effectiveness to I, but in the mixed out region there is little sensitivity. This is the first evidence of region dependence of the relative importance of different scaling parameters.

Specific Heat Capacity Flux Ratio. In this section, we consider the significance of the specific heat flux capacity ratio, E.

Results of RANS simulations for the binary region ($x = 0d$) are shown in Fig. 11 for test conditions $I = 1.000$, BR = 1.000, and TR = 0.800, and for values of E in the range $0.500 < E < 2.000$. In the binary region, the film effectiveness is essentially unaffected by the value of E. Here, the coolant flow is relatively unmixed, and changes in heat capacity flux have a small effect on the essentially binary value the film effectiveness takes.

Results for the intermediate region ($x = 24d$) are shown in Fig. 12. The peak in film effectiveness is enhanced from a value of approximately 0.25 to a value of approximately 0.55 as E is increased from 0.500 to 2.000. The average value of film effectiveness also increases in the same direction. As E increases (independent of the momentum flux ratio, blowing ratio, and temperature ratio), the relative (with respect to the mainstream) potential of the coolant to store heat is enhanced. Thus, for the same amount of heat transferred into the lower—cooler—layers of flow, the proportional temperature change is reduced.

The same effect is even more pronounced in the mixed-out region, where the balance of specific heat capacity fluxes (between coolant and mainstream) is the primary controlling parameter for the mixed-out temperature. This is shown in Fig. 13 ($x = 48d$). In this region, there is a relatively weak lateral variation in the film effectiveness, but a strong and approximately proportional relationship between the lateral mean value of the film effectiveness

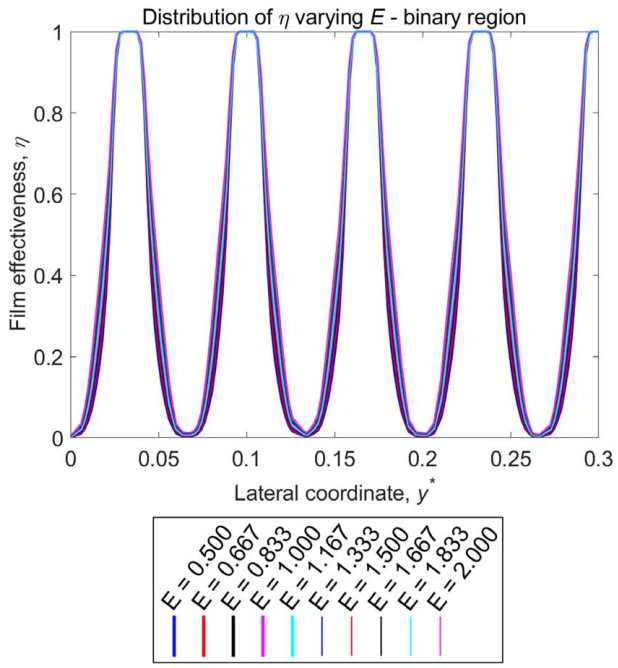

Fig. 11 Effect of specific heat capacity flux ratio on film effectiveness on the binary region ($x = 0d$). Test conditions were $I = 1.000$, BR = 1.000, and TR = 0.800.

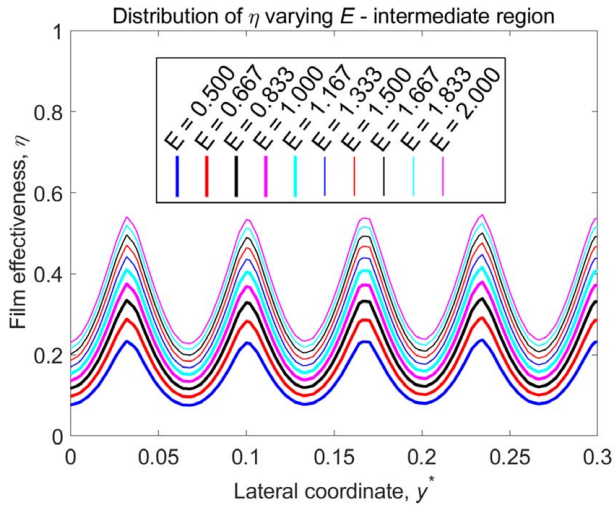

Fig. 12 Effect of specific heat capacity flux ratio on film effectiveness on the intermediate region ($x = 24d$). Test conditions were $I = 1.000$, BR = 1.000, and TR = 0.800.

and E. The mean value increases from approximately 0.10 to approximately 0.30 as E increases from 0.500 to 2.000.

Figure 14 shows the laterally averaged film effectiveness as a function of the specific heat capacity flux ratio for the three regions (binary, intermediate, and mixed-out), normalized with respect to the case of $E = 1.000$.

The dependence of film effectiveness on E is very weak in the binary region (variation less than 0.1 over the wide range of E). In the intermediate and mixed-out regions, a strong and approximately proportional dependence of the laterally averaged film effectiveness on E is observed: −0.4 to 0.55 in the intermediate region and −0.4 to 0.6 in the mixed out region.

In summary, in unmixed regions of flow, the balance of specific heat capacity flux is unimportant, because it has little effect on the approximately binary values the film effectiveness takes (here it is the structure of the flow that is important, as has been described). In contrast, where the flow is relatively mixed (in both the intermediate and mixed out regions) the relative heat storage capacity of the coolant and mainstream flows is important, and there is an approximately linear relationship between the laterally averaged film effectiveness and the heat capacity flux ratio.

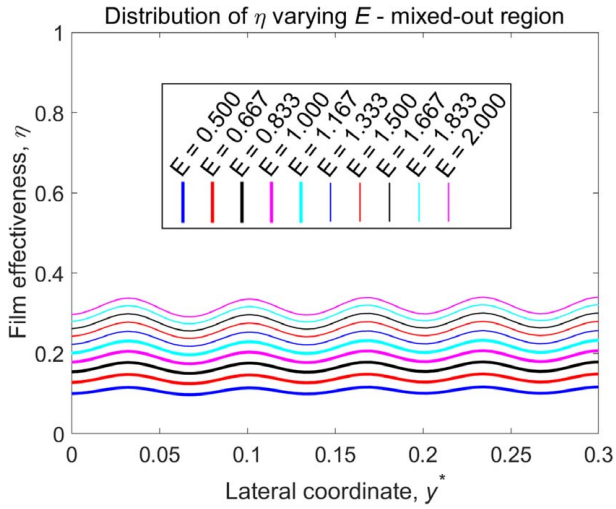

Fig. 13 Effect of specific heat capacity flux ratio on film effectiveness on the mixed-out region ($x = 48d$). Test conditions were $I = 1.000$, BR = 1.000, and TR = 0.800.

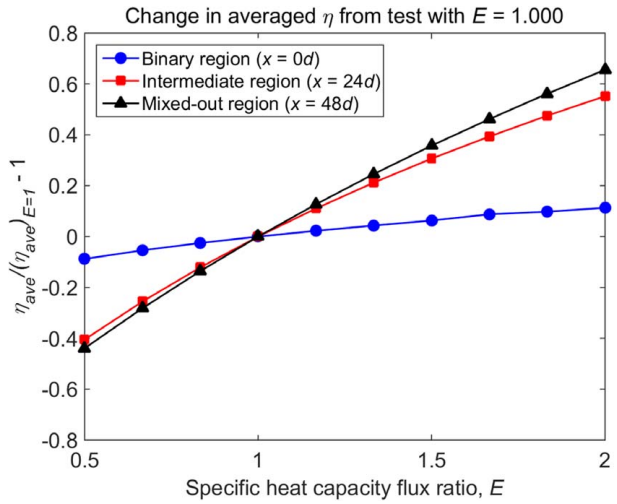

Fig. 14 Lateral average of film effectiveness as a function of *E*. Test conditions were *I* = 1.000, BR = 1.000, and TR = 0.800.

Blowing Ratio—Main Physical Processes. The blowing ratio describes the coolant-to-mainstream mass flux ratio for a given geometry. This is—in our view—a commonly used parameter in turbomachinery literature primarily because it relates to the input controls in an experiment (generally the mass flow is measured) or the cycle cost (aerodynamic and thermodynamic) in engine applications (generally directly proportional to the coolant mass flow), rather than because it has particularly useful physical significance in controlling the flow field. Indeed, it is relatively hard to understand what physical role this parameter plays when other non-dimensional parameters are held strictly constant, and, likewise, the sensitivity of the flow field to blowing ratio (when all other non-dimensional groups are held constant) is much lower than to other groups.

An important way in which the blowing ratio *does* differ from other non-dimensional parameters is in the way it describes the initial *volume flowrate ratio (VFRR)* or *velocity ratio* of the cooling jet with respect to the mainstream flow (when coolant is expanded to the local static pressure at the hole exit). The physical significance of the velocity ratio, in particular, is that it is directly related to the rate of shear at the interface between the emerging film cooling jet, and the mainstream flow. The shear at this interface causes the jet to destabilize, which affects the rate of mixing with the mainstream flow.

These ratios describe aspects of the film that are distinct from those described by the specific heat capacity flux ratio (a measure of the degree to which the film resists temperature change on mixing or heat exchange) or the momentum flux ratio (which determines trajectory). We, therefore, describe the blowing ratio in terms of the corresponding *volume flowrate ratio* or *velocity ratio*.

For a fixed momentum flux ratio, specific heat capacity flux ratio, and temperature ratio, the blowing ratio and volume flowrate ratio at the hole exit are inversely proportional. It follows that the velocity ratio is also inversely proportional to the blowing ratio. These slightly counter-intuitive results are derived in Appendix A. These relationships are shown in Fig. 15.

Figure 16 shows the tangential distribution of η as a function of the blowing ratio in the binary region ($x = 0d$). Across the blowing ratio range $0.500 < BR < 2.00$ the data collapse onto a single trend, indicating that there is essentially no sensitivity of film effectiveness to blowing ratio in the binary region.

Recalling that shear-induced destabilization of the jet tube is the main mechanism for mixing, this result is perhaps unsurprising for real flows or fully resolved simulated flows: in the vicinity of the hole exit the flow for all velocity ratios (or blowing ratios), the jet is not sufficiently destabilized for there to be a measurable difference between the cases. This will be discussed more in the context of LES simulations presented later in this section. So far as the RANS simulations are concerned, despite the lower fidelity of the modeling, a similar argument can be applied with respect to the shear-induced mixing of the flow (in this case introduced in the time-averaged flow via a turbulence model).

Figure 17 shows the tangential distribution of η as a function of the blowing ratio in the intermediate region. In this region, the film effectiveness is found to have a fairly significant dependence on the blowing ratio. The laterally averaged film effectiveness decreases for values between BR = 0.500 and BR = 0.833. For values above BR = 0.833 (BR = 1.000 upward), the film effectiveness increases monotonically. Although the complex trend is hard to explain,

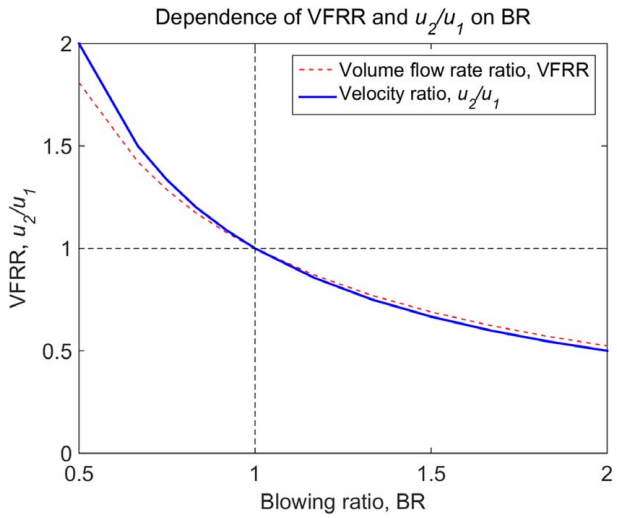

Fig. 15 Normalized volume flowrate ratio (normalized by the value at BR = 1) and absolute velocity ratio u_2/u_1 as a function of blowing ratio. Test conditions were *I* = 1.000, *E* = 1.000, and TR = 0.800.

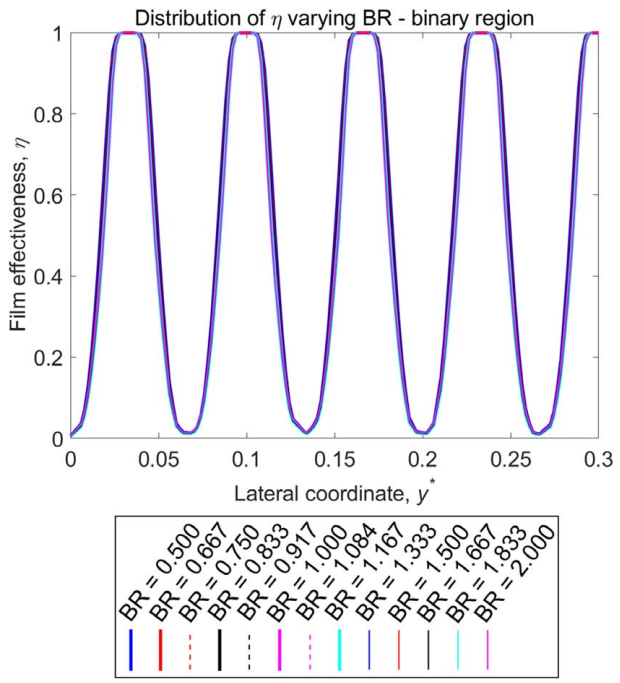

Fig. 16 Effect of blowing ratio on film effectiveness in the binary region ($x = 0d$). Test conditions were *I* = 1.000, *E* = 1.000, and TR = 0.800.

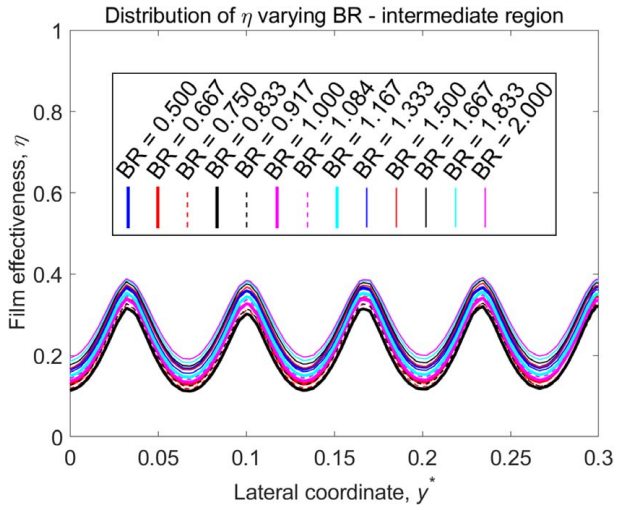

Fig. 17 Effect of blowing ratio on film effectiveness in the intermediate region ($x = 24d$). Test conditions were $I = 1.000$, $E = 1.000$, and TR = 0.800.

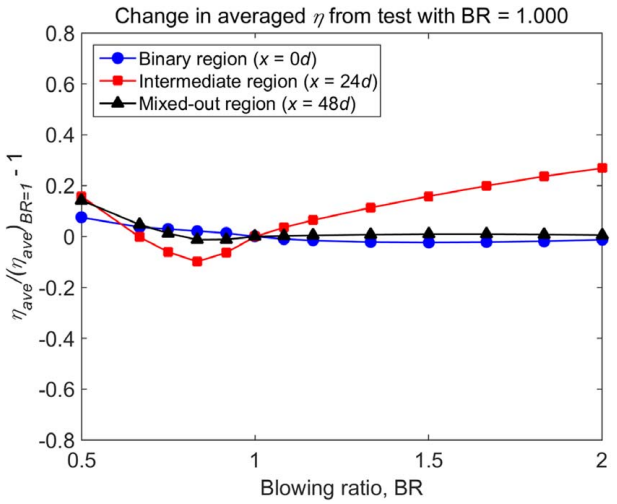

Fig. 19 Lateral average of film effectiveness as a function of blowing ratio. Test conditions were $I = 1.000$, $E = 1.000$, and TR = 0.800.

the fact that in there is significant dependence of η on BR in the intermediate region alone (and not in the binary region, or—as we will see—the mixed-out region) is consistent with the argument that shear-induced destabilization of the jet tube is the main mechanism for mixing. It is in the intermediate region that there is the onset of destabilization, and where there is the most rapid mixing of the coolant jet with the mainstream flow. The extent and nature of the shear-induced destabilization leads to complex flow effects which change the structure of the counter-rotating vortex pair, and lead to differences in the separation-reattachment behavior *for the same momentum flux ratio and same value of other non-dimensional parameters.* These complex phenomena are incompletely described with RANS modeling, but some of the driving mechanism (for example, shear leading to a counter-rotating vortex pair structure) are qualitatively captured. The mechanisms are discussed in more detail in Blowing Ratio—Structural Changes Caused by Shear section.

Figure 18 shows the effect of BR on the lateral film effectiveness distribution in the mixed-out out region ($x = 48d$). There is little sensitivity of film effectiveness to BR in this region. This is expected that the rate of shear in the mixed-out region is low, and structures

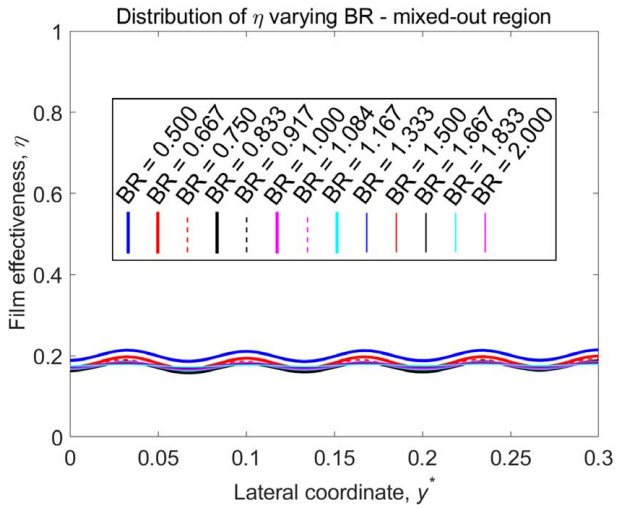

Fig. 18 Effect of blowing ratio on film effectiveness in the mixed-out region ($x = 48d$). Test conditions were $I = 1.000$, $E = 1.000$, and TR = 0.800.

generated by velocity differences in the upstream flow (in the intermediate region) have largely dissipated. Structurally speaking, the flow in the mixed out region is very insensitive to the blowing ratio.

Figure 19 shows laterally averaged film effectiveness as a function of blowing ratio, normalized with respect to a nominal condition at BR = 1.000. In the binary region, velocity difference driven shear forces have not yet taken hold, and there is little shear-induced structural difference between the flow fields. There is essentially no sensitivity of the laterally averaged film effectiveness to the blowing ratio across a wide range of conditions. In the mixed out region, we have the same result (almost no sensitivity of laterally averaged η to BR). Here, shear-induced destabilization has occurred some way upstream, and both the initial velocity discrepancy between coolant and mainstream and the structural differences generated by shear-initiated flow phenomena are largely mixed out. It is only in the intermediate region that there is significant sensitivity of laterally averaged η to BR. In the intermediate region, the normalized laterally averaged η varies between a minimum value of approximately −0.10 (BR = 0.833) and a maximum value of approximately 0.27 (BR = 2.000). In this region, shear-induced destabilization of the jet leads to complex flow structures that affect the rate of coolant jet and mainstream flow mixing and influence the way in which the mixing region interacts with the wall (extent and shape of bulk flow features like the counter-rotating vortex pair).

It is tempting to hypothesize that the reason the film effectiveness in the intermediate region rises either side of a minimum at approximate BR = 0.8 (see the trend in Fig. 19) is because this is a *minimum shear point*. Either side of this point, there is greater velocity discrepancy between the two flows, more rapid destabilization of the flow, greater mixing, and therefore the possibility of enhanced near-wall coolant flow in the partially mixed intermediate region. Indeed, with reference to Fig. 15, and noting that the lay angle of the holes with respect to the surface is 30 deg, the minimum velocity discrepancy point taking account of the hole angle is probably close to BR = 0.8. Although there is some reasonableness in this physical argument, it is not fully supported by all of the evidence. We believe the effect warrants further investigation, however.

Figure 20 shows visualizations (obtained with RANS simulations) of iso-surfaces at $\eta = 0.3$ for BR = 0.500, BR = 1.000, and BR = 2.000. The trajectory of the coolant "tubes" is similar for the three cases—a result that is expected because the momentum flux ratio is the same in these simulations. The "volumes" (what is visualized is the combined effect of the ejected volume flowrate ratio—see Fig. 15—and the mixing rate) of the tubes are different,

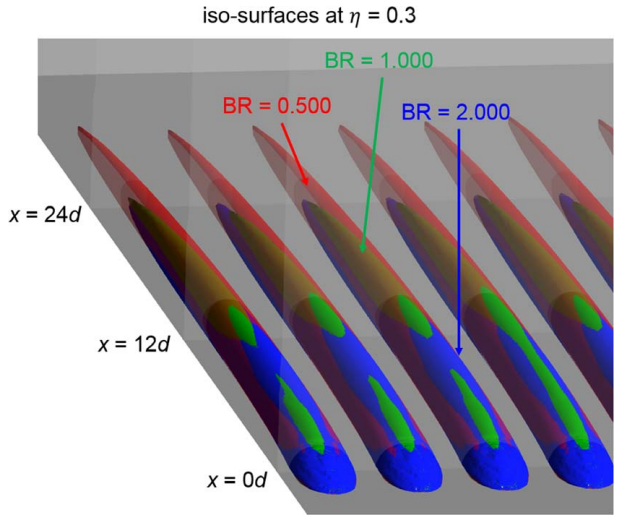

Fig. 20 Iso-surfaces at $\eta = 0.3$ for BR = 0.500, BR = 1.000, and BR = 2.000

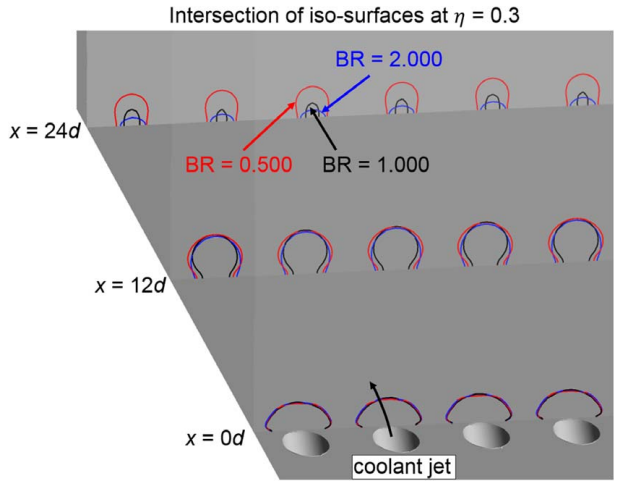

Fig. 21 Iso-lines at $\eta = 0.3$ at several axial planes for the cases with BR = 0.500, 1.000, and 2.000

however, with the volume of the BR = 0.500 case being substantially greater than for the BR = 1.000, consistent with the result of Fig. 15. The reduction in "volume" for the BR = 2.000 case (as compared with the BR = 1.000 case) is less evident, most likely because of shear-induced structural changes in the flow field, which affect the mixing.

As a thought experiment, we now consider the impact of volume flowrate changes on the "tube" containing the coolant.

At the hole exit, the jet cross section is determined by the hole area, angle, and momentum flux ratio—increased volume flowrate is carried by velocity excess within the tube (compared with the mainstream) rather than by an increased cross-sectional area of the tube. The effect of *friction* without mixing would be to gradually slow the tube to the velocity of the mainstream. As the velocity excess is reduced (eventually to zero), the tube cross-sectional area would increase. In the *fully accommodated state* (no velocity discrepancy with respect to the mainstream flow—i.e., a hypothetical case of the velocity accommodation through shear, without turbulent mixing) the cross-sectional area of the tube would take a ratio with respect to the nominal cross-sectional area equal to the normalized volume flowrate ratio presented in Fig. 15. That is for BR = 0.500, the cross-sectional area would be twice that of the baseline case (BR = 1.000), and for BR = 2.000, the cross-sectional area would be half that of the baseline case.

This argument is important for understanding the driving influence of the volume flowrate ratio, but in practice, this effect is conflated with two additional competing drivers. First, *even in the absence of turbulent mixing* (recall the thought experiment above), when higher-than-nominal (for example) volume flowrate ratio is achieved by decreasing the blowing ratio independent of other parameters, *the energy flux ratio within the tube remains the same as for the nominal case* (by definition). For a hypothetical tube for which velocities are fully accommodated and where the tube cross-sectional area has increased on account of the increased volume flowrate, but in which there is no turbulent mixing, the resistance of the tube contents to changes in temperature due to heat transfer are reduced (over given linear penetration distance) because the specific heat capacity flux per unit area in the tube is lower than the nominal case (by definition the specific heat capacity flux *within the tube* is the same as the nominal case). This effect tends to mitigate the impact of changes in volume flowrate (at both ends of the scale). The second effect is that higher-than-nominal (and, by the same token, lower-than-nominal) volume flowrate ratios have associated higher velocity differences (between coolant "tube" and mainstream flow) at the point of ejection into the mainstream flow. These velocity differences cause shear, which leads both to the destabilization of the jet and associated turbulent mixing, but also structural differences in the way the jet develops (extent of counter-rotating vortex pair, etc.). Naturally, these effects are extremely complex in nature.

Further visualizations of the flow are presented in Figs. 21 and 22 which show iso-lines of $\eta = 0.3$ and $\eta = 0.4$, respectively, at planes $x = 0d$, $12d$, and $24d$, for cases of BR = 0.500, BR = 1.000, and BR = 2.000.

At the coolant hole exit (binary region), the iso-lines of effectiveness for the three blowing ratios collapse to the same trend, indicating that the volume flow has essentially no effect in this region. This is consistent with the argument that at the hole exit, the jet cross section is determined by the hole area, angle, and momentum flux ratio, with an increased volume flowrate being carried by velocity excess within the tube.

In the intermediate region ($x = 12d$ and $x = 24d$), there is a significant change in both the tube size and shape with BR. Iso-lines for both $\eta = 0.3$ and $\eta = 0.4$ show substantially larger tube volume for BR = 0.500 compared with the case with BR = 2.000. The tube volumes for the BR = 1.000 and BR = 2.000 cases are more similar (in line with Fig. 15), and the trend is hard to distinguish when conflated with shear-driven structural changes in the flow. Notwithstanding caveats associated with structural changes in the flow field due to shear-stress differences, which are discussed in detail below, this is consistent with the general argument regarding the effect of *friction* without mixing. That is, as the tube is gradually slowed (in the case of velocity excess in the coolant, which occurs at lower BR), the tube cross-sectional area increases, and in the intermediate region (and also the mixed-out region, but in general other

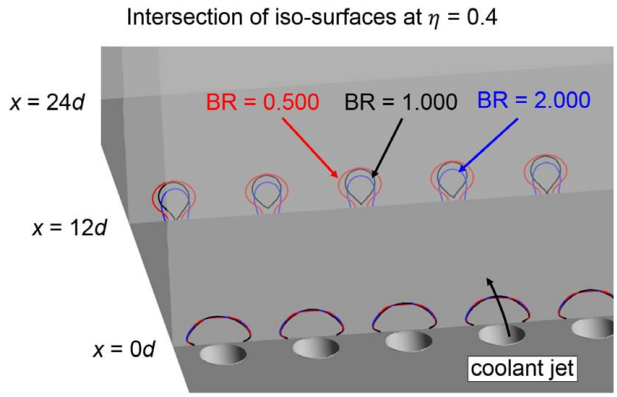

Fig. 22 Iso-lines at $\eta = 0.4$ at several axial planes for the cases with BR = 0.500, 1.000, and 2.000

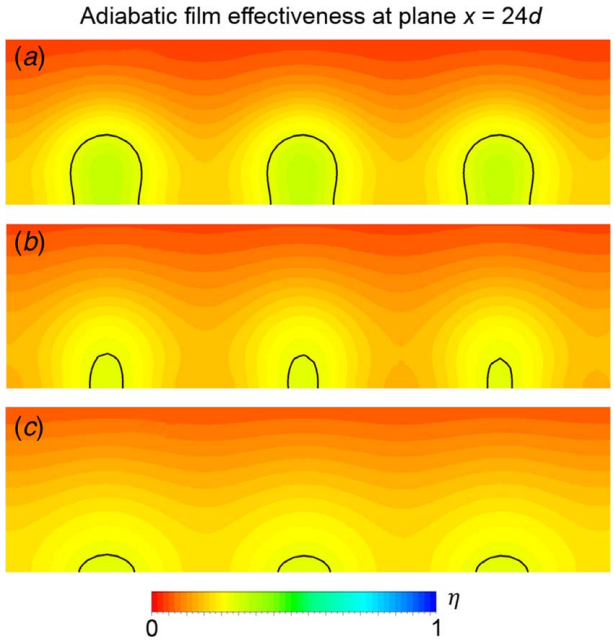

Fig. 23 RANS results of adiabatic film effectiveness distribution at $x = 24d$ for BR = 0.500, 1.000, and 2.000. Iso-lines at $\eta = 0.3$ are marked with a black line.

effects are overriding here) the tube cross-sectional areas are larger for lower BR due to the associated excess volume flowrate.

Figure 23 depicts the adiabatic film effectiveness distribution at $x = 24d$ (intermediate region) for BR = 0.500, 1.000, and 2.000. Iso-lines at $\eta = 0.3$ are marked in the figure. The distribution of η across the flow-normal plane is a strong function of BR, and this affects the lateral distribution at the wall. Although the trends agree with the results presented in Fig. 19 and demonstrate the effects of increased (at low BR) and decreased (at high BR) volume flowrate, the particular structures are not easy to explain, being the combined result of both volume changes in the mixing jet and shear-induced effects at the jet boundary, the latter leading to three-dimensional flow structures.

Blowing Ratio—Structural Changes Caused by Shear. Let us now consider how velocity differences caused by changes in blowing ratio introduce different shear profiles, which lead to structural differences in the flow field (changes in jet destabilization, the extent of counter-rotating vortex pair, etc.).

Figure 24 shows results from RANS simulations visualized by iso-level of Lambda-2 criterion for BR = 0.500, BR = 1.000, and BR = 2.000. Iso-lines with $\eta = 0.4$ (visible only up to $x = 12d$, before the jet mixes with the mainstream and η decays rapidly below 0.4) are also marked in the figure at the plane $x = 0d$ and $x = 12d$, for reference with Fig. 22. The RANS-predicted secondary flow structures are different for the different BR cases. The axial extent of the counter-rotating vortex decreases for increasing BR (from BR = 0.500 to BR = 2.000). It is clear that the shape of these, while difficult to explain from the contour pattern alone (e.g., Fig. 23) becomes clearer with reference to the full secondary flow field. When the full flow field is visualized, the complex behavior of the laterally averaged film effectiveness in the intermediate region (see Fig. 19) is not unexpected: it is here that there is most shear-induced secondary flow and associated mixing.

Figure 25 shows the laterally mass-averaged distribution of the shear strain rate as a function of normalized wall distance ($z^* = z/d$), for a number of blowing ratios, in the region where the jet first encounters the mainstream: $x = 0d$. It is clear from the figure that the BR has a significant impact on the development of the shear strain rate profile. As we hypothesized in relation to Fig. 15, the maximum shear strain rate at the outer edge of the

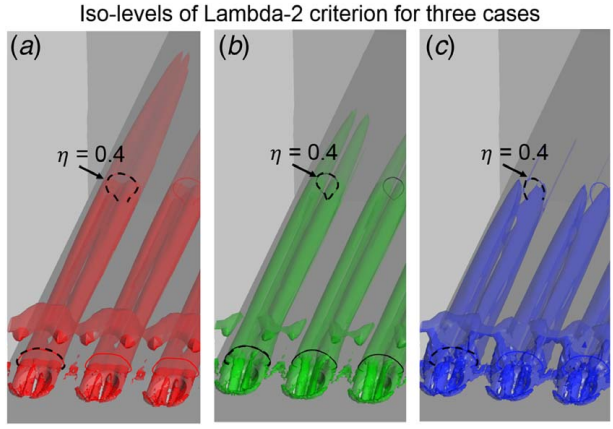

Fig. 24 Iso levels of Lambda-2 criterion for the case with BR = 0.500, 1.000, and 2.000. Iso-lines at $\eta = 0.4$ are also marked in the figures at planes $x = 0d$ and $x = 12d$, respectively.

mixing layer (for a given BR) is a strong function of the velocity discrepancy between the coolant and mainstream flows (for a given BR). This velocity discrepancy-induced shear is responsible for secondary flows, jet destabilization, and associated mixing effects. We now examine these effects.

We start by considering the case of BR = 1.000, for which the velocity ratio is $u_2/u_1 = 1.000$, and for which—by definition—the velocity discrepancy is zero (ignoring compound angle effects, which are relatively small). For this case, the shear strain rate profile decreases monotonically away from the wall (increasing z^*). The profile is typical of that for a boundary layer and is well-behaved with no peaks in the region of the coolant jet core (roughly between $0 < z^* < 0.6$). Excluding the high gradient region near the wall (laminar sublayer), the case of BR = 1.000 has the minimum shear strain of all the BR cases tested (0.500 < BR < 2.000). This is expected because the initial velocity discrepancy is zero (here we ignore relatively small effects due to angle variation).

For cases with BR > 1.000, there is an increasing velocity discrepancy (see Fig. 15) caused by relatively *slow* coolant flow. For the

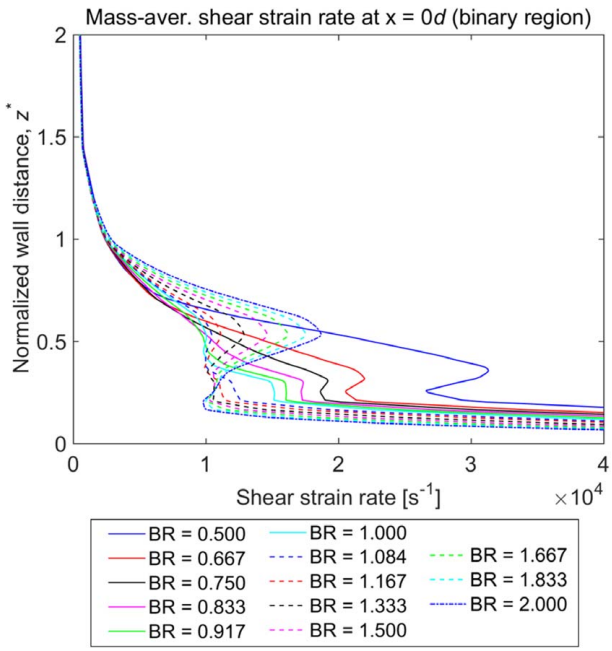

Fig. 25 RANS results of laterally mass-averaged shear strain rate profiles for various BR at plane $x = 0d$

highest case tested—BR = 2.000—the velocity discrepancy is equal to half the mainstream flow velocity. For all these cases, as BR increases, and as the corresponding velocity discrepancy increases, there is an increasing peak in shear strain rate in the region $0.25 < z^* < 1.0$. This is caused by shear on the outer surface of the jet tube. The approximate location of the peak in the shear strain rate is $z^* \approx 0.6$. The baseline value of the shear strain rate (BR = 1.000) is approximately $1 \times 10^4 s^{-1}$. For the highest case tested—BR = 2.000—the impact of velocity discrepancy is to increase the shear strain rate by $1 \times 10^4 s^{-1}$ to approximately $2 \times 10^4 s^{-1}$.

For cases with BR < 1.000, there is an increasing velocity discrepancy (see Fig. 15) caused by relatively *fast* coolant flow. For the lowest case tested—BR = 0.500—the velocity discrepancy is equal to the mainstream flow velocity (i.e., twice the velocity discrepancy for the BR = 2.000 case). Similarly to the previous cases, as BR decreases, and as the corresponding velocity discrepancy *increases*, there is an increasing peak in shear strain rate in the region $0.25 < z^* < 0.8$. For the lowest case tested—BR = 0.500—the impact of velocity discrepancy is to increase the shear strain rate by 2×10^4per s to approximately 3×10^4per s. The increase in shear strain rate is almost exactly twice that for the BR = 2.000 case. This is quantitatively as expected because the velocity discrepancy is twice the magnitude of the BR = 2.000 case.

We summarize this extended discussion in the conclusions.

Temperature Ratio. In this section, we consider the effect of changing TR, T_{02}/T_{01}, when all other groups (10 of 11 in total) are held constant, including the blowing ratio, momentum flux ratio, and specific heat capacity flux ratio. To achieve variation in TR while maintaining the other groups constant, it is necessary to vary both T_{02} and R_2. The constraints on the system lead to the following interesting results, which are proven, and discussed in some detail, in Appendix B:

(i) The density of the coolant film at the point of issuing from the hole is *not* a function of TR.
(ii) The density of a *partially mixed* layer of coolant decreases (from a maximum at TR = 1) for temperature ratios *either side of unity*.
(iii) A consequence of (ii) is that the kinematic viscosity increases from a minimum at TR = 1, *either side of a TR of unity* leading to higher momentum diffusivity for both TR > 1 and TR < 1 than for TR = 1. It is worth noting that the constraints on the system mean that dynamic viscosity, which is a fluid property, remains constant with TR.
(iv) A second consequence of (ii) is that the exit-to-inlet volume flowrate ratio across a mixing domain containing the film and a fraction of entrained mainstream gas increases from a minimum at TR = 1, *either side of a TR of unity*. This is equivalent to volume dilation during the mixing process. For TR > 1 and TR < 1, this effect acts to push flow structures—including turbulent structures—further into the main flow than would be the case for TR = 1.

Results (ii), (iii), and (iv) are particularly interesting and have significant consequences for the behavior of the mixing film. The results are not intuitive, and the reader is referred to Appendix B for derivations of the results and discussion. The results are developed by way of a control volume approach, and while they are initially counter-intuitive, they are in extremely good agreement (both qualitatively and quantitatively) with the LES results that follow.

We now examine LES results for the following temperature ratios: 0.350, 0.950, 1.520, and 1.995. In these studies, blowing ratio, momentum flux ratio, and specific heat capacity flux ratio were kept constant, as were the remaining 10 of 11 (in total) nondimensional groups for this problem. As we will see, the results for the mixing layer (as opposed to boundary layer) density ratio, volume flowrate ratio, and kinematic viscosity ratio are in good agreement with the results from the control volume method.

Figure 26 shows instantaneous ($t = 2$ ms) vortex structures (Lambda-2 criterion, with Lambda value equal to 4.4×10^6 per s^2) for LES for cases with TR = 0.350, 0.950, 1.520, and 1.995. The structures are colored by the normalized distance from the wall (z^*). The size of turbulent structures (and the intensity, measured by Reynolds stress) increases either side of a TR of unity. This is the result of two effects, volume dilation of the mixing layer either side of TR = 1, and an increase in kinematic viscosity either side of TR = 1, driven by a reduction in density either side of TR = 1. The size and intensity of turbulent structures by visually ranking the images is, in descending order of intensity, TR = 0.350, TR = 1.995, TR = 1.520, and TR = 0.950. This ranking is precisely consistent with the kinematic viscosity ratio (increase in momentum

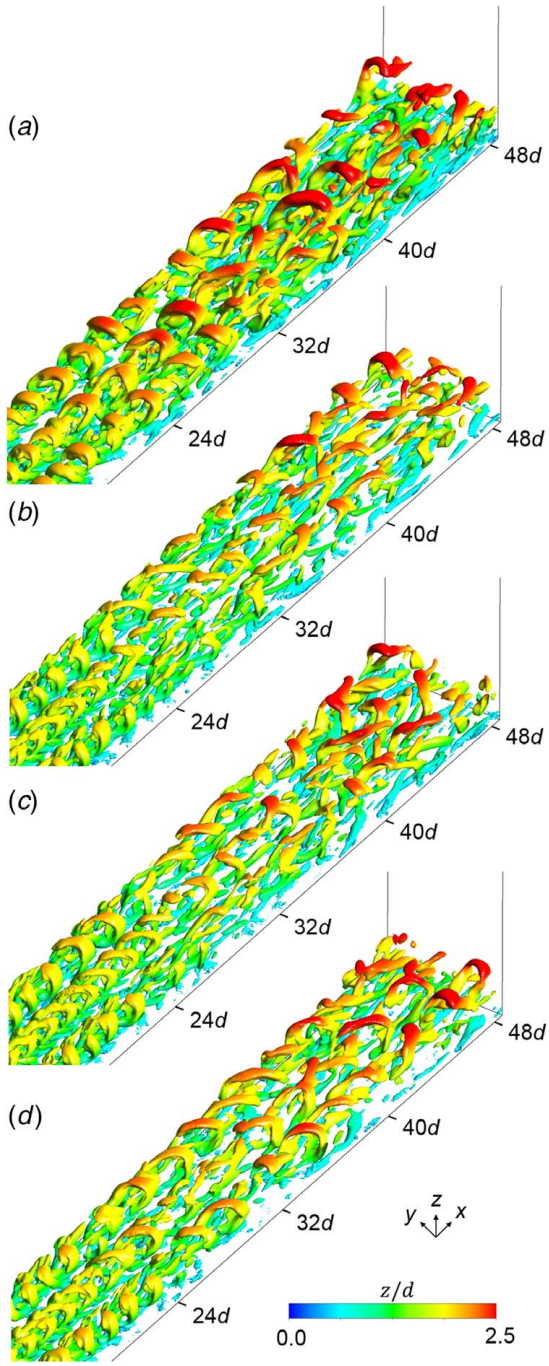

Fig. 26 LES instantaneous vortex structures (Lambda-2 criterion) with contours of normalized distance from the wall (z^*): (*a*) TR = 0.350, (*b*) TR = 0.950, (*c*) TR = 1.520, and (*d*) TR = 1.995

diffusivity in the flow) and volumetric flowrate ratio (dilation effect) ranking presented in Appendix B. This is a satisfying qualitative (the visualizations of Fig. 26) and semi-quantitative result.

The laterally averaged axial distributions of film effectiveness corresponding to the LES plot of Fig. 26 are shown in Fig. 27. As expected, solutions for both TR > 1 and TR < 1 have effectiveness distributions lower than for the case with TR = 0.950 (i.e., TR ≈ 1), on account of the enhanced kinematic viscosity ratio *both sides* of TR = 1. Indeed, the ranking of results is pleasingly consistent with the ranking of the kinematic viscosity ratios in Appendix B: that is, the magnitude of the deficit in film effectiveness in Fig. 27 (greatest for TR = 0.350, followed by 1.995 followed by 1.520) is ordered according to the surplus in kinematic viscosity (Appendix B). It is worth noting that there is some sensitivity of the kinematic viscosity ratio in the mixing layer to the mixing ratio, $\dot{m}_2/\dot{m}_1$, which *decreases* with axial distance as the film effectiveness reduces. This kinematic viscosity ratio is a function both of the density variation with mixing ratio and temperature ratio (see results in Appendix B) and a direct function of the mass balance of input dynamic viscosities (noting that μ_1 and μ_2 are different).

We now consider changes in the flow with respect to wall-normal distributions of density and Reynolds stress.

Figure 28 shows LES-predicted mass-averaged distributions of time-averaged density ratio in the partially mixed cooling layer (ρ_3/ρ_1) as a function of normalized wall distance at planes $x = 0d$, $24d$, and $48d$, for TR = 0.350, 0.950, 1.520, and 1.995. Here, the temperature ratio is defined at the hole exit ($x = 0d$).

In accordance with our result (ii)—full argument in Appendix B—for a temperature ratio close to unity (TR = 0.950), the density ratio at all axial planes is approximately unity. For temperature ratios *either side of unity*, however, the density of the partially mixed layer decreases from a maximum for TR = 1. The reduction in density in the partially mixed layer depends on both the TR and also the degree of mixing (ratio of entrained mainstream gas to coolant gas in the partially mixed layer). It is worth recalling that the density ratio *at the hole exit* is unity for all values of TR.

Looking at the trends in Fig. 28, we see that for all stations ($x = 0d$, $24d$, or $48d$) the maximum reduction in density is achieved for TR = 0.350. This is consistent with the result of Appendix B. For $x = 0d$, the degree of entrainment of mainstream flow is small, with a correspondingly small reduction in density ratio. For $x = 24d$ and $x = 48d$, the entrainment of mainstream flow is greater, and a more significant reduction in density ratio is seen. For $x = 24d$, the reduction is from $\rho_3/\rho_1 = 1.00$ to $\rho_3/\rho_1 = 0.85$ in the region $0 < z^* < 2$. For $x = 48d$, the results are very similar,

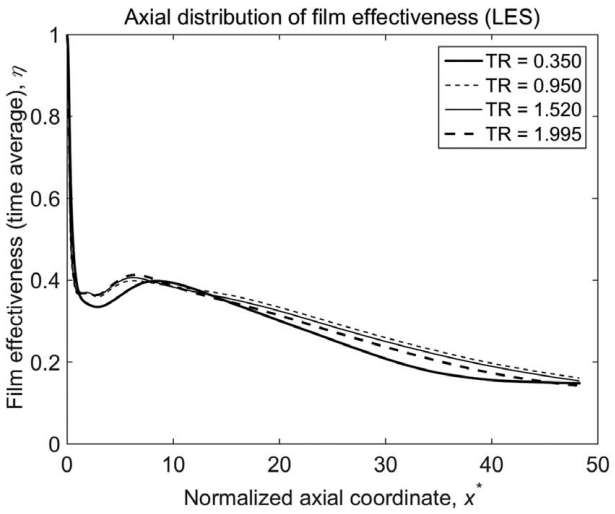

Fig. 27 Laterally averaged axial distributions of time-averaged film effectiveness for LES simulations TR = 0.350, 0.950, 1.520, and 1.995

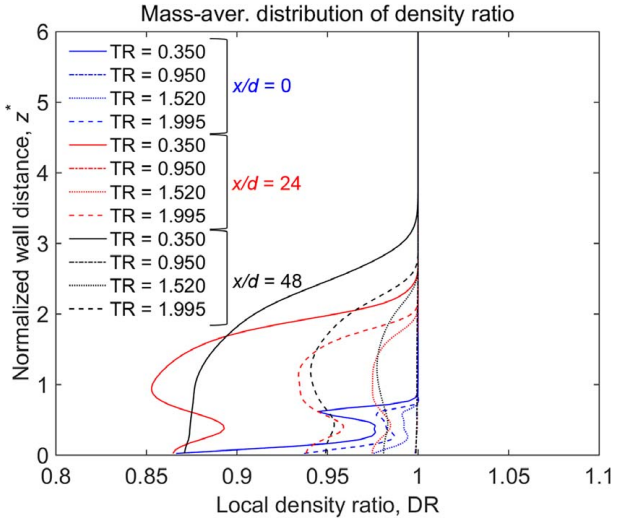

Fig. 28 LES results of mass-averaged time-averaged density ratio distribution at plane x = 0, 24, and 48*d*

with a maximum density reduction to $\rho_3/\rho_1 = 0.87$, with most of the effect localized in the region $0 < z^* < 3$. Similar trends, but with decreasing magnitude, are observed for TR = 1.995 and TR = 1.520, respectively. This ranking is in accordance with the results of Appendix B.

In interpreting these results, it is worth noting that the density ratio in the mixing layer (ρ_3/ρ_1) is a *weak* function of the mixing ratio which *decreases* with axial distance (Appendix B) as the film effectiveness reduces. The general effect is that for greater x/d, the film effectiveness is lower due to a lower mixing ratio, $\dot{m}_2/\dot{m}_1$, due to more entrained mainstream gas. At x/d equal to 24 and 48 (intermediate and mixed-out regions), the mixing ratios are approximately $\dot{m}_2/\dot{m}_1 = 0.3$ and $\dot{m}_2/\dot{m}_1, = 0.2$, respectively. The inference from the data presented in Appendix B (trend line shown for $\dot{m}_2/\dot{m}_1 = 0.5$, but not directly for 0.3 or 0.2) is that the low mixing ratios ameliorate the temperature ratio dependent density reduction effect by about an order of 0.01 (from the maximum at a mixing ratio of $\dot{m}_2/\dot{m}_1 = 1$).

Temperature ratio induced reductions in density in the mixing layer (Appendix B) cause a corresponding increase in the kinematic viscosity. This increase is observed *either side of a TR of unity* leading to higher momentum diffusivity for both TR > 1 and TR < 1 than for TR = 1. This is for a system in which both the dynamic viscosity and density ratio at hole exit are constant for all temperature ratios.

Figure 29 shows LES-predicted mass-averaged distributions of the $\overline{uu'}$ component of Reynolds stress as a function of normalized wall distance for $x = 0d$, $24d$, and $48d$.

For $x = 0d$ where there has been relatively little mixing between the coolant and mainstream, and relatively little shear-induced destabilisation of the flow, the $\overline{uu'}$ component of Reynolds stress is similar for all temperature ratios and takes a low value. Further downstream, where the flow has been destabilized and there has been substantial mixing between coolant and mainstream, the Reynolds stress increases, and is significantly affected by temperature ratio induced density changes. At $x = 24d$, there is a peak in Reynolds stress within the mixing layer (between $0 < z^* < 2$), with peak magnitude ranked according to the temperature ratio induced change in density within the mixing layer. That is, the greatest enhancement in Reynolds stress due to temperature ratio effects is observed for TR = 0.350, followed by TR = 1.995. The Reynolds stress profiles for TR = 1.520 and TR = 0.950 are essentially indistinguishable. It is interesting to note that the Reynolds stress enhancement for the TR = 0.350 case extends further from the wall then for the other cases, consistent with a volume dilation effect within the mixing layer.

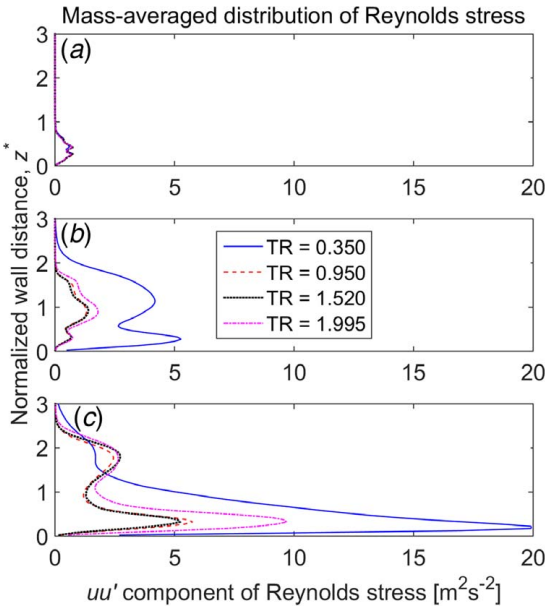

Fig. 29 LES predictions of the mass-averaged $\overline{uu'}$ component of Reynolds stresses, along the normalized wall distance at planes $x = 0$, 24, and 48d

Similar trends are observed at $x = 48d$. Here the peak stresses are higher than at $x = 24d$ (perhaps consistent with continuing growth in turbulent structures downstream of the cooling holes), and the ranking of enhancement in Reynolds stress over the baseline case (TR = 0.950) due to temperature ratio effects is consistent with the results at $x = 24d$, and in line with the density variation discussed in Appendix B.

Figure 30 shows laterally averaged film effectiveness as a function of temperature ratio, normalized with respect to a nominal condition at TR = 0.950.

In the binary region, the impact of temperature ratio is extremely small, and there is very little difference between cases for TR = 0.350, 0.950, 1.520, and 1.995. This is perhaps to be expected, because the three physical effects discussed (see the start of this section) develop as the coolant entrains mainstream gas (leading to density variations, and subsequent volume dilation effects and changes in kinematic viscosity). At $x = 0d$, although both coolant and mainstream gas are present on the surface (discreet cooling jets with gaps between), effects due to mixing (see control volume argument in Appendix B) have not yet been initiated. In the intermediate region ($x = 24d$), there is a very small reduction in film effectiveness either side of TR = 1. The general shape of this relationship (a maximum at TR = 1) is consistent with the general principle that the key physical processes have the same sign either side of TR = 1. The small reduction in effectiveness is most likely due to enhanced kinematic viscosity (either side of TR = 1) leading to faster (momentum-based) diffusion between the coolant and entrained mainstream layers. This can be seen in Fig. 29, which shows larger and more intense turbulent structures for TR < 1 and TR > 1 than for TR = 1.

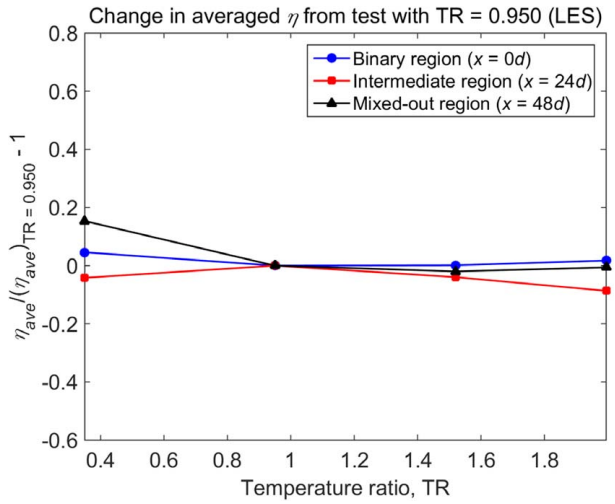

Fig. 30 Lateral average of film effectiveness as a function of temperature ratio. Test conditions were $I = 1.000$, $E = 1.000$, and BR = 1.000.

In the mixed-out region ($x = 48d$), there is a very small increase in film effectiveness for TR = 0.350 (note that these data are presented as proportional changes, and the underlying value is small). The data at TR = 0.950, 1.520, and 1.995 are extremely similar to each other. There is a suggestion of a minimum in the data that simulations at more extreme conditions could explore. If such a minimum exists, it would be consistent with the argument that the physical processes take the same sign either side of TR = 1. Noting that the underlying value of film effectiveness is small, it is speculated that the increase in film effectiveness may be due to volume dilation effects (maximum for the TR = 0.350 condition) in an already fully turbulent and well-mixed coolant region reducing the penetration of freestream turbulent structures into the mixed layer (due to the mixed layer assuming greater thickness on account of volume dilation, in relation to the length scale of turbulent structures in the mainstream flow). This hypothesized mechanism is not believed to be robust and would benefit from further investigation at more extreme temperature ratios, in which the rate of entrainment into various segmented near-wall regions could be analyzed.

Conclusions

By conducting a dimensional analysis of a flow field with a mixing coolant film, we have shown that the situation is governed by 12 non-dimensional groups. Making film effectiveness the subject, we can show that seven of the remaining 11 groups can be regarded as boundary conditions for the main flow path—and must be matched for complete similarity—and the remaining four relate specifically to the introduction of film cooling. We believe there is lack of clarity in the literature both about the best form for these groups (they can be cast in numerous ways), and about the *independent* role they play in determining the film effectiveness distribution in a given situation. We argue that the most natural (that is, the forms that allow the clearest physical interpretation of *independent* effects; or, mathematically speaking, make the axes as orthogonal as possible) forms for groups on which the film effectiveness has a strong functional dependence are

(i) the momentum flux ratio, $I \equiv \rho_2 u_2^2/\rho_1 u_1^2$;
(ii) the blowing ratio, $\mathrm{BR} \equiv \rho_2 u_2/\rho_1 u_1$;
(iii) the heat capacity flux ratio, $E = \rho_2 u_2 c_{p2}/\rho_1 u_1 c_{p1}$;
(iv) the temperature ratio, $\mathrm{TR} \equiv T_{02}/T_{01}$.

With the aid of extensive RANS and LES predictions, we independently vary each of these four groups while keeping the remaining three groups—and an additional seven groups associated with the bulk flow field—constant. This enabled the independent effect of each group to be studied.

An important observation that departs from previous literature is that we see strong *region dependence* of the sensitivity of the film effectiveness to each of these four parameters. We define three regions for analysis: a *binary region* in which the films are essentially unmixed; an *intermediate region* in which the films are partially mixed; and a *mixed-out region* in which the films are well mixed. The key results of these four studies (one per controlling non-dimensional group) are now summarized in turn.

Momentum Flux Ratio. In the binary region, we find the film effectiveness distribution has a strong dependence on the momentum flux ratio, because this controls the aerodynamic state of the jets, i.e., the coolant trajectory and shape of the jet. This result is consistent with a large body of literature. In the intermediate region, there is still significant dependence on the film effectiveness distribution on the momentum flux ratio. This is beyond the reattachment point of the jets, so the sensitivity is likely associated with changes in mixing caused by different initial coolant trajectories. We find that in the mixed out region, the film effectiveness is insensitive of the momentum flux ratio. This shows the importance of region-dependent analysis, which departs from most literature in this area which generally only extends to discussing the relative dominance of particular groups in holistic terms. In addition, there are many examples in the literature of studies of this type in which groups are not properly separated from each other.

Blowing Ratio. In our view, this a commonly used parameter in turbomachinery literature primarily because it relates to the input controls in many experiments, or the cycle cost (aerodynamic and thermodynamic) in engine applications. We find, however, that the relatively subtle physical processes this parameter controls are not those discussed in existing literature, and further observe that the sensitivity of film cooling to blowing ratio (when varied on its own) is much lower than to other non-dimensional parameters. Indeed, in much of the literature, changes in film effectiveness which should correctly be attributed to energy flux ratios changes are incorrectly attributed to blowing ratio changes. Although there is less sensitivity of film cooling to blowing ratio than to other parameters, we have shown that blowing ratio is responsible for describing the initial *volume flowrate ratio* or *velocity ratio* of the cooling jet with respect to the mainstream flow (when coolant is expanded to the local static pressure at the hole exit). The velocity ratio governs the rate of shear at the interface between the emerging film cooling jets and the mainstream flow, which in turn dictates the rate of jet destabilization, which affects the rate of mixing of coolant with the mainstream flow. We therefore believe that thinking of the blowing ratio as controlling initial (near-hole exit) velocity ratio (or velocity difference) provides the most intuitive explanation of the resulting physical effects. For fixed momentum flux ratio, specific heat capacity flux ratio, and temperature ratio, the velocity ratio and corresponding volume flowrate ratio are inversely proportional to blowing ratio, a counter-intuitive result that is proved in this paper. Changes in blowing ratio cause three complex, competing effects: velocity excess/deficit in the coolant tube is accommodated by friction leading to increased/decreased tube cross-sectional area in the fully accommodated state; tube area expansion/reduction due to volume flowrate changes is offset by a reduced/increased resistance to temperature change (over a given linear distance) because the tube-specific heat capacity flux remains unchanged; both velocity excess and deficit cause shear, which leads to jet destabilization, turbulent mixing, and structural differences in the way the jet develops. By examining shear strain rate profiles along the wall-normal direction in RANS simulations, we see that the last effect is extremely complex in nature. Although the effects are competing, and complex, the sensitivity of laterally averaged effectiveness to blowing ratio is relatively low. In the binary region, velocity difference driven shear forces have not yet taken hold, and there is little shear-induced difference in the flow. Here, sensitivity of η to BR is negligible. In the mixed-out region, we have the same result (almost no sensitivity of laterally averaged η to BR). Here, shear-induced destabilization has occurred some way upstream, and both the initial velocity discrepancy between coolant and mainstream and the structural differences generated by shear-initiated flow phenomena are largely mixed out. It is only in the intermediate region that there is some sensitivity of laterally averaged η to BR. This is attributed to complex flow structures (resulting from shear-induced destabilization) affecting the rate of coolant jet and mainstream flow mixing.

Heat Capacity Flux Ratio. The heat capacity flux ratio is a measure of the relative (with respect to the mainstream) potential of the coolant stream to store heat. In the binary region, where the flow is essentially unmixed, the balance of specific heat capacity flux is unimportant, because it has little effect on the approximately binary values the film effectiveness takes (here it is only the structure of the flow that is important). In the intermediate and mixed-out regions where the flow is relatively well mixed, the relative heat storage capacity of the coolant and mainstream flows is extremely important, and there is an approximately linear relationship between the laterally averaged film effectiveness and the heat capacity flux ratio. In these regions, the film effectiveness is more sensitive to this parameter than any other. It is worth noting that in the literature there are many examples of sensitivity to specific heat capacity flux ratio being incorrectly attributed to changes in blowing ratio. To conflate these two sensitivities is entirely wrong and should be avoided.

Temperature Ratio. A change in temperature ratio alone does not cause a change in density (or density ratio) of the coolant film at the point of issuing from the hole, but, interestingly, does cause a change in the density of a *partially mixed* layer of coolant. A key result is the density of such a layer decreases (from a maximum at TR = 1) for temperature ratios *either side of unity*. There are two consequences of this effect: first, the kinematic viscosity increases *either side of a TR of unity* leading to higher momentum diffusivity and greater mixing within the near-wall region; second, there is a volume dilation effect during the mixing process (of coolant gas with entrained mainstream). These effects appear to be opposed in terms of their impact on the film effectiveness: the kinematic viscosity increase appears to enhance early mixing of the film, leading to slightly lower film effectiveness in the intermediate region either side of a temperature ratio of unity; the volume dilation may be responsible for slowing the entrainment of mainstream gas in the mixed out region (length scale ratio of turbulent structure to mixed layer), but further study is required to validate this hypothesis. There is no impact on the binary region, consistent with the argument that the effects are driven by density variation in a *partially* mixed layer.

The purpose of this paper was to bring clarification to the following topics: the full set of non-dimensional groups that control film cooling problems; the way in which the groups *independently* control features of the flow, and the form of groups that allows clearest physical interpretation; the strong region dependence of the sensitivity of film effectiveness to certain groups; and the physical mechanisms that lead to changes in film effectiveness when blowing ratio, momentum flux ratio, specific heat capacity flux ratio, and temperature ratio are independently varied. A number of fundamentally new mechanisms and concepts have been discussed that we hope will be referenced by future studies, either by way of further validating or challenging our theses.

Acknowledgment

The support of Rolls Royce Plc is gratefully acknowledged. The authors would like also to acknowledge the use of the University of Oxford Advanced Research Computing (ARC) facility.[2]

Nomenclature

Acronyms

BR = blowing ratio, $(\rho_2 u_2)/(\rho_1 u_1)$
DR = density ratio, ρ_2/ρ_1
VR = velocity ratio, u_2/u_1

[2]http://dx.doi.org/10.5281/zenodo.22558

Roman Symbols

d = hole diameter, m
f = frequency, Hz
k = thermal conductivity, W/(m K)
p = pressure, Pa
s = streamwise coordinate, m
t = time, s
u = velocity component along x, m/s
v = velocity component along y, m/s
w = velocity component along z, m/s
x = streamwise coordinate, m
y = lateral coordinate, m
z = distance from the wall, m
E = specific heat capacity flux ratio, $(\rho_2 u_2 c_{p2})/(\rho_1 u_2 c_{p1})$
I = momentum flux ratio, $(\rho_2 u_2^2)/(\rho_1 u_1^2)$
L = characteristic length, m
M = Mach number
R = specific gas constant, J/(kg K)
T = static temperature, K
U = velocity, m/s
$\dot{m}$ = mass flowrate, kg/s
$\dot{V}$ = volume flowrate, m^3/s
c_p = heat capacity, J/(kg K)
x^* = normalized axial location ($x^* = x/d$)
x^+ = normalized streamwise distance based on Re
y^* = normalized tangential location ($y^* = (y - y_{min})/(y_{max} - y_{min})$)
y^+ = normalized lateral distance based on Re
z^* = normalized wall distance ($z^* = z/d$)
z^+ = normalized wall distance based on Re
$\overline{uu'}$ = uu component of the Reynolds stress tensor, m^2/s^2
Pr = Prandtl number
Re = Reynolds number
St = Strouhal number
Tu = turbulent intensity

Greek Symbols

γ = isentropic exponent (heat capacity ratio)
ε = turbulent dissipation rate, m^2/s^3
η = adiabatic film cooling effectiveness
κ = Kolmogorov's length scale, m
μ = dynamic viscosity, Pa s
ν = kinematic viscosity, m^2/s
π_i = dimensionless group
ρ = density, kg/m^3

Subscripts

0 = total conditions
1 = mainstream gas conditions
2 = coolant conditions
w = conditions at the wall
x = component along x axis
y = component along y axis
z = component along z axis

Appendix A: Demonstration that Velocity Ratio and Volume Flowrate Ratio are Inversely Proportional to Blowing Ratio when Varying Blowing Ratio Alone

In this section, we demonstrate the slightly counter-intuitive result that for fixed momentum flux ratio, fixed specific heat capacity flux ratio, and fixed temperature ratio, and in experiments in which the inlet total pressure and external aerodynamics are fixed (see text relating to Eq. (14)), the velocity ratio and volume flowrate ratio are inversely proportional to blowing ratio.

Consider Eq. (6), repeated here for convenience

$$\mathrm{BR} \equiv \frac{\rho_2 u_2}{\rho_1 u_1} = \left(I \frac{\rho_2}{\rho_1}\right)^{1/2} = \left(\frac{p_{02}}{p_{01}} \frac{T_{01}}{T_{02}} \frac{c_{p1}}{c_{p2}} \frac{\gamma_2}{\gamma_1} \frac{\gamma_1 - 1}{\gamma_2 - 1} \frac{p_{02} - p}{p_{01} - p}\right)^{1/2} = \pi_2 \tag{6}$$

Constant temperature ratio by definition means the term (T_{02}/T_{01}) is constant. As we have noted, for incompressible flow, constant momentum flux ratio implies constant $(p_{02} - p)/(p_{01} - p)$. In our CFD experiments, we arbitrarily fix p_{01} and the domain exit static pressure (note that this leave sufficient freedom to adjust our non-dimensional groups as required). The domain geometry is fixed, and therefore this leads to fixed local static pressure, p, at the cooling hole exit. These boundary conditions are the same as many real experiments with fixed external aerodynamics. Constant $(p_{02} - p)/(p_{01} - p)$, constant p_{01}, and constant p necessarily imply constant p_{02} and therefore constant p_{02}/p_{01}.

Let us now return to Eq. (6). For the constraints we have specified, there are two remaining degrees-of-freedom

$$\frac{\gamma_2}{\gamma_1} \frac{\gamma_1 - 1}{\gamma_2 - 1} \tag{A1}$$

$$c_{p1}/c_{p2} \tag{A2}$$

Recalling Eq. (7), $E = \mathrm{BR}(c_{p2}/c_{p1})$, fixed specific heat capacity flux ratio implies a proportional relationship between c_{p1}/c_{p2} and BR. Noting the square root on all terms on the right-hand side of Eq. (6), noting the result $c_{p1}/c_{p2} \propto \mathrm{BR}$, and noting there are only two degrees of freedom with the specified constraints (terms A1, A2), we see that the term A1 must also be proportional to BR. That is

$$\gamma_2/\gamma_1(\gamma_1 - 1)/(\gamma_2 - 1) \propto c_{p1}/c_{p2} \propto \mathrm{BR} \tag{A3}$$

Using Meyer's relation

$$\gamma_2/\gamma_1(\gamma_1 - 1)/(\gamma_2 - 1)(c_{p1}/c_{p2}) = R_1/R_2 \tag{A4}$$

therefore

$$R_1/R_2 \propto \mathrm{BR}^2 \tag{A5}$$

Taking the ideal gas law, $p/\rho = RT$, noting that for incompressible flow $p_0 \approx p$ and $T_0 \approx T$, recalling that in all of the studies in this paper we arbitrarily fixed T_{01} (see text related to Eq. (15)), and that in this study in particular (varying blowing ratio alone) we have fixed T_{01}/T_{02}, we obtain, for this study

$$\rho \propto 1/R \tag{A6}$$

Combining (A5) and (A6)

$$\mathrm{BR}^2 \propto \rho_2/\rho_1 \tag{A7}$$

Therefore as BR increases, ρ_2/ρ_1 will increase as the square of BR. For fixed I, recalling Eq. (4) ($I = \rho_2 u_2^2/\rho_1 u_1^2$), the ratio u_2^2/u_1^2 will be inversely proportional to BR. That is, $u_2/u_1 \propto 1/\mathrm{BR}$. *The velocity ratio and volume flowrate ratio are inversely proportional to the blowing ratio.*

Appendix B: Demonstration that for Coolant-to-Mainstream Temperature Ratios Either Side of Unity There is a Reduction in Density in the Mixing Layer, and an Associated Increase Both in Kinematic Viscosity and in the Volume of the Mixing Layer

In this section, we demonstrate the result that for fixed momentum flux ratio, fixed blowing ratio, and fixed specific heat capacity flux ratio, and in experiments in which the inlet total pressure and

external aerodynamics are fixed, that for coolant-to-mainstream temperature ratios *either side* of unity, there is a *decrease* in the density ratio of the flow in a partially mixed out film, and an associated increase both in kinematic viscosity and in the volume of the mixing layer.

Consider the form of the non-dimensional groups we intend to keep constant, I, E, and BR

$$I \equiv \frac{\rho_2 u_2^2}{\rho_1 u_1^2} = \frac{p_{02} - p}{p_{01} - p} \tag{B1}$$

$$E = \frac{\rho_2 u_2 c_{p2}}{\rho_1 u_1 c_{p1}} = \mathrm{BR}\frac{c_{p2}}{c_{p1}} \tag{B2}$$

$$\mathrm{BR} \equiv \frac{\rho_2 u_2}{\rho_1 u_1} = \left(\left(\frac{p_{02}}{p_{01}}\right)\left(\frac{T_{01}}{T_{02}}\right)\left(\frac{c_{p1}}{c_{p2}}\right)\left(\frac{\gamma_2}{\gamma_1}\frac{\gamma_1 - 1}{\gamma_2 - 1}\right)\left(\frac{p_{02} - p}{p_{01} - p}\right)\right)^{1/2} \tag{B3}$$

To keep I constant (equation (B1)), we required fixed inlet total pressure (p_{01}) and external aerodynamics (p), and additionally fixed coolant total pressure, p_{02} To keep E constant (equation (B2)), noting that BR must also be kept constant in this study, we required constant c_{p1}/c_{p2}. Finally, to keep BR constant (equation (B3)), and noting that first, third, and fifth terms in the right-hand parentheses are constant (required for constant I and E), and further noting that we are varying term two (by definition, as variation of temperature ratio—alone—is the purpose of this study), we observe that the fourth term, $(\gamma_2/\gamma_1)(\gamma_1 - 1)/(\gamma_2 - 1)$, is inversely proportional to T_{01}/T_{02}. It is possible to show that $(c_{p1}/c_{p2})(\gamma_2/\gamma_1)(\gamma_1 - 1)/(\gamma_2 - 1) = R_1/R_2$. Thus, for constant c_{p1}, c_{p2}, and R_1 (constraints that meet our requirements in this study), we see that $T_{01}/T_{02} \propto 1/(R_1/R_2)$ or $R_2 \propto 1/(T_{02}/T_{01}) \equiv 1/\mathrm{TR}$). This result is plotted in Fig. 31. A consequence of the inverse proportionality of R_2 and T_{02} is that ρ_2 is constant (for incompressible flow) with varying T_{02} or TR. This is also shown in Fig. 31.

Figure 31 shows the required variation in R_2 (normalized by R_1, which is constant with TR) to maintain constant values of I, E, and BR while varying TR. We now consider the impact of this variation in R_2 on the behavior of partially mixed coolant film. Consider the control volume of Fig. 32, which we will use to examine the behavior of a partially mixed film.

We want to consider the changes in behavior with TR within the mixing film, and to do this we arbitrarily pick a mixing ratio $\dot{m}_1/\dot{m}_2 = 1$. We define a bounding streamline as the line that

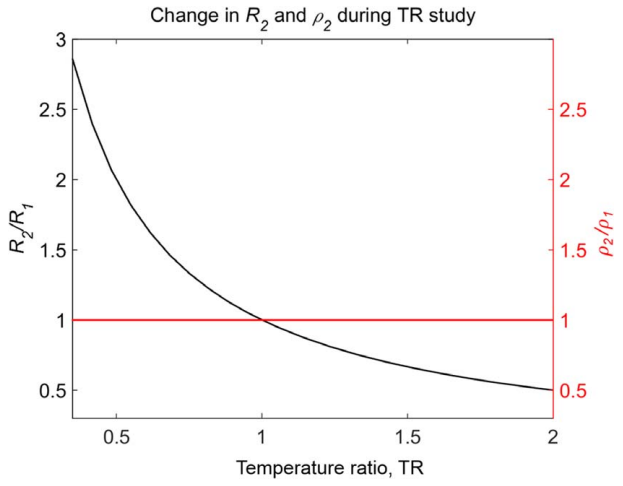

Fig. 31 Variation of coolant gas constant R_2 (normalized by R_1, which is constant with TR), and coolant gas density ρ_2 (normalized by ρ_1, which is constant with TR) as a function of temperature ratio

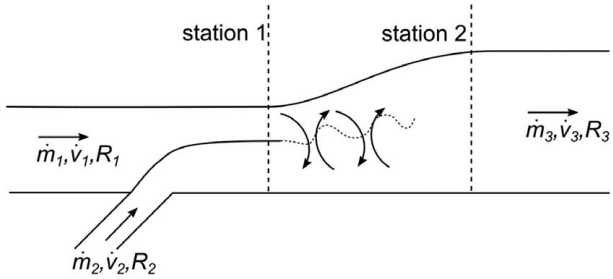

Fig. 32 Control volume for a partially mixed coolant film

contains these two streams of equal mass flux. We define the boundary conditions for the mixing process as follows:

(i) Constant static pressure along the bounding streamline;
(ii) No heat transfer across the bounding streamline.

At the inlet state, station 1, the two flows are entirely unmixed. At the outlet state, station 2, the two flows are fully mixed. We note that the (mass) continuity condition and constraint that $c_{p1} = c_{p2}$ means that at station 2 the equivalent adiabatic film effectiveness is 0.5.

It is worth noting that for constant BR (in our varying TR study), and for the same flow structure (dictated by I in the region close to the hole) the mass flowrate (per unit domain width) distributions with wall-normal distance through station 1 do no vary with TR. That is, the position of the hypothetical bounding streamline that preserves the condition $\dot{m}_2/\dot{m}_1 = 1$ does not change with TR. Likewise, for constant I, the distribution with wall-normal distance of *volume flowrate per unit domain width* is unchanged with varying TR. In fact, for all values of TR, the nominal values $\mathrm{BR} = 1$ and $I = 1$ imply $\dot{V}_1 = \dot{V}_2$, for our arbitrarily selected $\dot{m}_2 = \dot{m}_1$. In summary, the mass flowrates and volume flowrates into the control volume at station 1 are unchanged with changing TR.

We now consider what happens in the process of fully mixing the flows between station 1 and station 2. The mixed out total temperature T_{03} is determined by the energy and (mass) continuity equations

$$\dot{m}_1 c_{p1} T_{01} + \dot{m}_2 c_{p2} T_{02} = \dot{m}_3 c_{p3} T_{03} \tag{B4}$$

$$\dot{m}_1 + \dot{m}_2 = \dot{m}_3 \tag{B5}$$

where we note in general that $c_{p3}\dot{m}_3 = c_{p1}\dot{m}_1 + c_{p2}\dot{m}_2$, but in our special case $c_{p1} = c_{p1} = c_{p3}$. For our special case, the mixed-out temperature at station 2 is given by

$$T_{03} = (\dot{m}_1 T_{01} + \dot{m}_2 T_{02})/\dot{m}_3 \tag{B6}$$

Likewise, the mixed-out specific gas constant at station 2 is

$$R_3 = (R_1 \dot{m}_1 + R_2 \dot{m}_2)/\ \dot{m}_3 \tag{B7}$$

For constant T_{01} and R_1, the resulting variations in T_{03} and R_3 (normalized by T_{01} and R_1) with TR are presented in Fig. 33. The mixed out temperature T_{03} increases linearly with T_{02} (and therefore TR). The mixed out specific gas constant R_3 is quasi-inversely proportional to T_{02} (and therefore TR). This is explained (via equation B6) by the constant value of R_1, the precisely inverse relationship between R_2 and TR (Fig. 31) and the fixed ratio $\dot{m}_2/\dot{m}_1 = 1$.

We now consider the consequences of the trends T_{03}(TR) and R_3(TR) for the mixed out density, ρ_3, and the corresponding volumetric flowrate out of the control volume, $\dot{V}_3$.

The mixed out density obeys the ideal gas law, $\rho_3 = p_3/R_3 T_3$, and noting both that the mixing process occurs at constant static pressure ($p_1 = p_2 = p_3$) and that the flow is to a good approximation incompressible ($T_3 \approx T_{03}$ and $\rho_3 \approx \rho_{03}$), the function that ρ_3 takes with TR, ρ_3(TR), is dictated by the trends T_{03}(TR) and R_3(TR) in

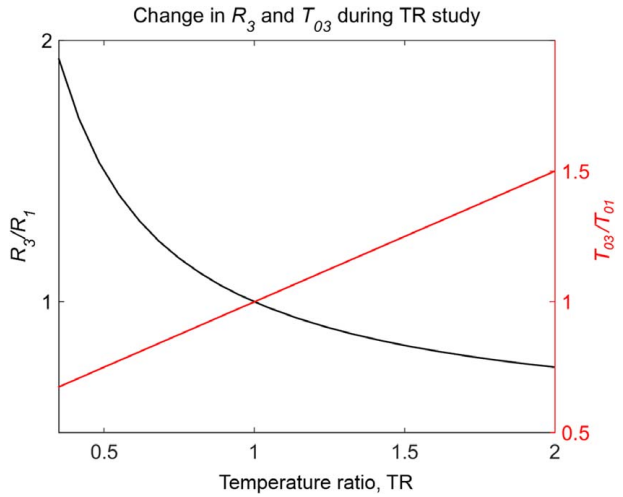

Fig. 33 Variation of R_3 (normalized by R_1, which is constant with TR) and T_{03} (normalized by T_{01}, which is constant with TR) as a function of TR

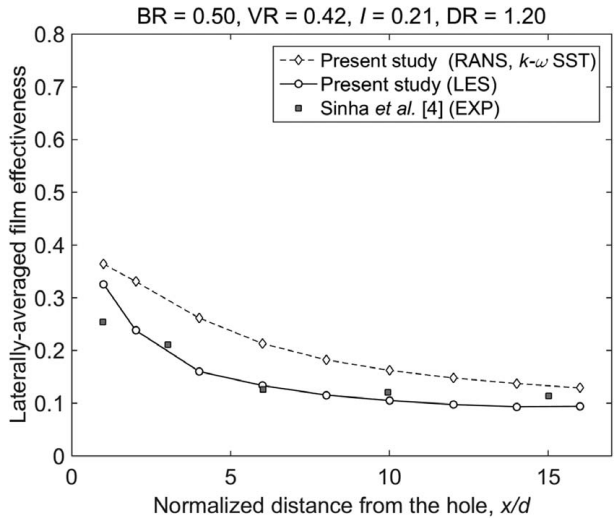

Fig. 35 Laterally averaged film effectiveness as a function of normalized distance from the hole: RANS simulations, LES simulations, and experimental data from Sinha et al. [4]

Fig. 33 (these are presented normalized by the constant values T_{01} and R_1). These trends are such that the resulting mixed out density *decreases for temperature ratios either side of unity*. The trend is shown in Fig. 34. The important result is perhaps surprising, and has interesting implications that are discussed in the main body of this paper. The most significant of these results is that *kinematic viscosity increases either side of a temperature ratio of unity*, or equivalently there is higher momentum diffusivity in the mixing layer either side of unity (note that the dynamic viscosity, which is a fluid property, is constant). The variation with temperature ratio of the kinematic viscosity of the partially mixed layer (normalized by the kinematic viscosity of the coolant at the point of injection, ν_2) is shown in Fig. 34. Results are shown for mixing ratios $\dot{m}_2/\dot{m}_1 = 0.5$, 1.0, and 2.0.

Now we ask what happens to the volume flowrate ratio $\dot{V}_3/(\dot{V}_1 + \dot{V}_2)$ across the domain (i.e., between unmixed station 1, and fully mixed station 2). We recall that the inlet mass flowrates are equal to each other, and constant with varying TR, and that inlet volume flowrates, $\dot{V}_1$ and $\dot{V}_2$, are equal to each other and constant with varying TR. It follows that the output mass flowrate is constant with varying TR. The output density varies as shown in Fig. 34, however. The result is that *the volume flowrate ratio increases either side of a TR of unity* (see Fig. 34). This is equivalent to volume dilation in the mixing layer, which pushes flow structures—including turbulent structures—further into the main flow than would be the case for TR = 1. This second significant result is discussed in the main body of the paper.

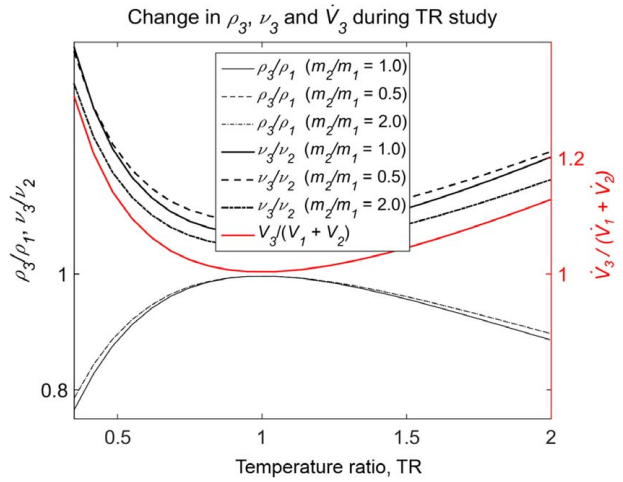

Fig. 34 Variation with TR of density ratio of the partially mixed layer ρ_3/ρ_1; volume flowrate ratio of the partially mixed layer $\dot{V}_3/(\dot{V}_1 + \dot{V}_2)$; kinematic viscosity ratio of the partially mixed layer ν_3/ν_2

Appendix C: Validation of Numerical Methods

In this section, we present validation of the RANS (with k–ω SST turbulence model) and LES methods that were used in this work. This section is reconciled to an appendix because absolute accuracy of the predictions is of only of second-order interest for our present purpose: in this paper, we are primarily concerned with fundamental physical effects in the mixing region, and what this implies in terms of the non-dimensional representation of data. As we have no specific interest in any particular geometry, our primary concern is the conservative nature of the CFD methods (inherent in essentially all methods), and the ability to model physical processes relevant to particular effects discussed in the paper (different for RANS and LES).

Validation simulations were performed for the experimental geometry and conditions reported by Sinha et al. [4], which is—in terms of the geometry used—the most similar experimental study to the present work. The geometry had a hole inclination angle of 35 deg and a hole spacing of 3d.

Results from both RANS and LES simulations were compared with experimental results in terms of laterally averaged film effectiveness for the case with BR = 0.5, I = 0.21, VR = 0.42, and DR = 1.20. Figure 35 shows comparisons of the three data sets. RANS simulations with the k–ω SST turbulence model show good agreement in terms of the trend of film effectiveness, but significantly over-predict the absolute level (by about 40% just downstream of the hole exit, decaying to approximately 25% at $x/d = 16$). This is in accord with the well-known tendency of RANS models to under-predict both streamwise and lateral mixing of film cooling. The LES simulations agree very well with the experimental data and accurately capture both the trend and absolute level in laterally averaged film effectiveness.

References

[1] Eckert, E. R. G., 1992, "Similarity Analysis of Model Experiments for Film Cooling in Gas Turbines," Wärme—und Stoffübertragung, **27**(4), pp. 217–223.

[2] Baldauf, S., and Scheurlen, M., 1996, "CFD Based Sensitivity Study of Flow Parameters for Engine Like Film Cooling Conditions," ASME Paper 96-GT-310.

[3] Luque, S., Jones, T. V., and Povey, T., 2016, "Theory for the Scaling of Metal Temperatures in Cooled Compressible Flows," Int. J. Heat Mass Transfer, **102**, pp. 331–340.

[4] Sinha, A. K., Bogard, D. G., and Crawford, M. E., 1991, "Film Cooling Effectiveness Downstream of a Single Row of Holes With Variable Density Ratio," ASME J. Turbomach., **113**(4), pp. 442–449.
[5] Thole, K. A., Sinha, A. K., and Bogard, D. G., 1990, "Mean Temperature Measurements of Jets With a Crossflow for Gas Turbine Film Cooling," Proceedings of the Third International Symposium on Transport Phenomena and Dynamics of Rotating Machinery (ISROMAC-3), Honolulu, HI, Apr. 1–4, pp. 69–85.
[6] Haas, W., Rodi, W., and Shonung, B., 1991, "The Influence of Density Difference Between Hot and Coolant Gas on Film Cooling by a Row of Holes: Predictions and Experiments," ASME J. Turbomach., **114**(4), pp. 747–755.
[7] Bogard, D. G., and Thole, K. A., 2006, "Gas Turbine Film Cooling," J. Propul. Power, **22**(2), pp. 249–270.
[8] Pedersen, D. R., Eckert, E., and Goldstein, R., 1977, "Film Cooling With Large Density Differences Between the Mainstream and the Secondary Fluid Measured by the Heat-Mass Transfer Analogy," ASME J. Heat Transfer, **99**(4), pp. 620–627.
[9] Shiau, C. C., Chen, F. C., Han, J. C., Azad, S., and Lee, C. P., 2016, "Full-Scale Turbine Vane Endwall Film Cooling Effectiveness Distribution Using Pressure-Sensitive Paint Technique," ASME J. Turbomach., **138**(5), p. 051002.
[10] Prost, J. W., and Acharya, S., 2010, "The Role of Density Ratio and Blowing Ratio on Film Cooling in a Vane Passage," ASME Paper GT2010-23680.
[11] Vinton, K. R., Watson, T. B., Wright, L. M., Crites, D. C., Morris, M. C., and Riahi, A., 2016, "Combined Effect of Freestream Pressure Gradient and Density Ratio on the Film Cooling Effectiveness of Round and Shaped Holes on a Flat Plate," ASME Paper GT2016-56210.
[12] Rutledge, J. L., and Polanka, M. D., 2014, "Computational Fluid Dynamics Evaluations of Unconventional Film Cooling Scaling Parameters on a Simulated Turbine Blade Leading Edge," ASME J. Turbomach., **136**(10), p. 101006.
[13] Rutledge, J. L., Polanka, M. D., and Greiner, N., 2017, "Computational Fluid Dynamics Evaluations of Film Cooling Flow Scaling Between Engine and Experimental Conditions," ASME J. Turbomach., **139**(2), p. 021004.
[14] Greiner, N., Polanka, M. D., and Rutledge, J. L., 2015, "Scaling of Film Cooling Performance From Ambient to Engine Temperatures," ASME J. Turbomach., **137**(7), p. 071007.
[15] Nicoud, F., and Ducros, F., 1999, "Subgrid-Scale Stress Modelling Based on the Square of the Velocity Gradient Tensor," Flow Turbul. Combust., **62**(3), pp. 183–200.
[16] Tyacke, J. C., and Tucker, P. G., 2015, "Future Use of Large Eddy Simulations in Aero-Engines," ASME J. Turbomach., **137**(8), p. 081005.
[17] Tyacke, J. C., Tucker, P. G., Jefferson-Loveday, R., Rao Vadlamani, N., Watson, R., Naqavi, I., and Yang, X., 2013, "Large Eddy-Simulations for Turbines: Methodologies, Costs, and Future Outlooks," ASME J. Turbomach., **136**(6), 061009.
[18] Lin, X. C., Liu, J. J., and An, B. T. (2016). "Calculation of Film-Cooling Effectiveness and Aerodynamic Losses Using DES/SAS and RANS Methods and Compared With Experimental Results," ASME Paper GT2016-89477.